Endothelial FGF signaling is protective in hypoxia-induced pulmonary hypertension

Kel Vin Woo,[1,2] Isabel Y. Shen,[2] Carla J. Weinheimer,[3] Attila Kovacs,[3] Jessica Nigro,[3] Chieh-Yu Lin,[4] Murali Chakinala,[5] Derek E. Byers,[5] and David M. Ornitz[2]

[1]Division of Cardiology, Department of Pediatrics, [2]Department of Developmental Biology, [3]Cardiovascular Division, Department of Medicine, [4]Department of Pathology and Immunology, and [5]Division of Pulmonary and Critical Care Medicine, Department of Medicine, Washington University School of Medicine, St. Louis, Missouri, USA.

Hypoxia-induced pulmonary hypertension (PH) is one of the most common and deadliest forms of PH. Fibroblast growth factor receptors 1 and 2 (FGFR1/2) are elevated in patients with PH and in mice exposed to chronic hypoxia. Endothelial FGFR1/2 signaling is important for the adaptive response to several injury types and we hypothesized that endothelial FGFR1/2 signaling would protect against hypoxia-induced PH. Mice lacking endothelial FGFR1/2, mice with activated endothelial FGFR signaling, and human pulmonary artery endothelial cells (HPAECs) were challenged with hypoxia. We assessed the effect of FGFR activation and inhibition on right ventricular pressure, vascular remodeling, and endothelial-mesenchymal transition (EndMT), a known pathologic change seen in patients with PH. Hypoxia-exposed mice lacking endothelial FGFRs developed increased PH, while mice overexpressing a constitutively active FGFR in endothelial cells did not develop PH. Mechanistically, lack of endothelial FGFRs or inhibition of FGFRs in HPAECs led to increased TGF-β signaling and increased EndMT in response to hypoxia. These phenotypes were reversed in mice with activated endothelial FGFR signaling, suggesting that FGFR signaling inhibits TGF-β pathway–mediated EndMT during chronic hypoxia. Consistent with these observations, lung tissue from patients with PH showed activation of FGFR and TGF-β signaling. Collectively, these data suggest that activation of endothelial FGFR signaling could be therapeutic for hypoxia-induced PH.

Introduction

Pulmonary hypertension (PH) is a severe form of pulmonary vascular disease that results in death in up to two-thirds of affected patients within 5 years of diagnosis. There are 5 World Health Organization subtypes of PH. Group 3 PH, the second deadliest category of PH, is caused by hypoxemia resulting from developmental lung disorders such as bronchopulmonary dysplasia (BPD), chronic obstructive lung disease (COPD), combined pulmonary fibrosis and emphysema (CPFE), interstitial lung disease, alveolar hypoventilation disorders, or high altitude (1, 2).

PH increases the morbidity and mortality in patients with COPD, BPD, and CPFE (3–5). Preterm birth affects more than 500,000 babies born in the United States each year and BPD is the most common complication in preterm infants born before 29 weeks of gestation (3). Up to half of preterm infants with BPD and PH die within 2 years of diagnosis (3). Five to ten percent of patients with COPD are diagnosed with PH, and up to 64% of these patients will die within 5 years (4, 6). First described by Cottin et al., CPFE is characterized by a history of heavy smoking, exercise hypoxemia, upper lobe emphysema, lower lobe fibrosis, abnormally low lung volumes, and severely reduced carbon monoxide transfer (7). Between 47% and 90% of patients with CPFE develop PH (6, 8) and most will develop moderate to severe PH (9).

PH contributes to the dysfunction of patients with CPFE including severe dyspnea, markedly impaired transfer of gas, and exercise hypoxemia, ultimately resulting in a poorer prognosis (10). An estimated 1-year survival rate of 60% was reported in patients with both CPFE and PH (8).

PH is characterized by pathologic changes in endothelial cell (EC) and vascular wall function. In response to pathologic stimuli such as hypoxia, hyperplasia of vascular smooth muscle (VSM) increases pulmonary vascular pressure (11–15). EC dysfunction, excessive vascular remodeling, and inflammation contribute to progressive elevation of pulmonary vascular resistance, leading to increased right ventricular (RV) afterload. The histopathology of PH is well documented, but the molecular mechanisms underlying the vascular remodeling are poorly understood.

Sustained increase in RV afterload ultimately results in right heart failure. Current pharmacological treatments focused on vasodilation for symptomatic relief have limited effects on vascular remodeling. Research has led to drugs that have significantly decreased morbidity and prolonged life expectancy in patients with Group 1 PH. Only some of these drugs show benefit to patients with Group 3 PH (6, 16, 17). A mechanistic understanding of the pulmonary vascular remodeling in Group 3 PH is thus necessary to identify noninvasive diagnostic tools for early detection of cardiopulmonary compromise, to develop effective therapies, to monitor treatment response, and to improve overall outcome.

Endothelial-mesenchymal transition (EndMT) is a form of cellular plasticity described as the ability of ECs to dedifferentiate into a multipotent mesenchymal progenitor. EndMT begins with a morphological change from a classical cobblestone-like structure

JCI

to an elongated, spindle shape. The process further undergoes a loss of cell-cell adhesion, dissociation from the basement membrane, and migration into the medial layer. EndMT is involved in normal vascular development and several pathologies, including pulmonary arterial hypertension (PAH, also known as Group 1 PH), atherosclerosis, and tumor angiogenesis (18–20). EndMT is regulated by a common set of physiological effectors, including hypoxia, inflammation, and shear stress (21), and molecular effectors, including transforming growth factor β (TGF-β) and fibroblast growth factor (FGF) (19). Inflammation facilitates EndMT in a TGF-β–dependent manner (11), and shear stress downregulates FGF receptor (FGFR) signaling and enhances nuclear localization of TGF-β–activated Smad2/3 (21). EndMT is characterized by reduced production of EC proteins such as platelet EC adhesion molecule-1 (PECAM1, CD31) and vascular endothelial cadherin (VE-cadherin, CDH5), accompanied by a concomitant increase in production of mesenchymal markers such as α-smooth muscle actin (αSMA, ACTA2), fibronectin (FN1), and vimentin (VIM) (22).

The TGF-β family consists of a group of multifunctional cytokines that signal via type 1 and type 2 Ser/Thr kinase receptors and Smad transcription factors (23). Upon TGF-β activation, receptor-regulated Smad2 and Smad3 become phosphorylated, translocate to the nucleus, and in combination with other transcription factors regulate gene expression. TGF-β–induced phosphorylated-Smad2/3 (p-Smad2/3) nuclear accumulation is enhanced by hypoxic conditions (24). TGF-β2 stimulates EndMT by signaling through canonical Smad2/3 and noncanonical pathways (18). Activation of the Smad2/3 pathway leads to overexpression of Twist (TWIST1 and TWIST2), Snail (SNAI1), and Slug (SNAI2) transcription factors (25–27). The TWIST family are a group of helix-loop-helix transcription factors that can bind DNA E-boxes to regulate transcription (28). Among the EndMT target genes upregulated by hypoxia, SNAI1 was identified as a master regulator (29). The SNAI1 family of zinc finger transcription factors share a highly conserved C-terminal region required for transcriptional repressor activity and a posttranslationally modifiable central domain that can regulate protein stability or localization (30). TGF-β–mediated EndMT can also be modulated by FGF signaling through FGFRs and the adaptor molecule FRS2. Knocking down FRS2 in human umbilical vein endothelial cells (HUVECs) caused an increase in the production of αSMA and vimentin (31). Independent of TGF-β, loss of BMPR2 can also induce gene expression changes consistent with EndMT (32). TGF-β has been shown to induce EndMT in PAH (20); however, its role in Group 3 PH has not been established.

FGF2 and FGFR1/2 protein levels are elevated in lung tissue samples from patients with PH (33–35). Additionally, FGF2 is elevated in a mouse model of Group 3 PH where mice are exposed to chronic hypoxia (36, 37) and in vitro in human ECs cultured under hypoxic conditions (38). Changes in the expression of both ligand and receptors suggest that there may be functional consequences of this signaling pathway in the pathogenesis of PH. To study the role of FGFR signaling in ECs in vivo, mouse models have been generated that lack EC FGFR1 and FGFR2 (39, 40). Studies of these mice show that EC FGFR1 and FGFR2 are dispensable for mouse embryonic development and are not required for vascular

or hematopoietic homeostasis; however, when challenged with skin, retina, or ischemia-reperfusion heart injury, mice lacking EC FGFR1/2 displayed impaired neovascular growth and tissue repair (39, 40). Additionally, loss of EC FGFR1 activity caused increased neointimal thickness in a vein graft model (41). Studies investigating the role of FGFR signaling in EndMT have demonstrated interactions between FGFR and TGF-β signal transduction pathways (42). Hence, we hypothesize that EC FGFR1/2 signaling promotes EC signals that protect against PH.

To investigate the function of EC FGFR signaling in the pathogenesis of PH, we examined the response of mice lacking EC FGFR1/2 or mice in which EC FGFR1 signaling was activated through 2 weeks of chronic hypoxia. We found that mice deficient in EC FGFR signaling developed more severe PH, whereas mice in which FGFR1 signaling was activated in ECs developed less severe PH. Furthermore, we show that the lack of EC FGFR1/2 signaling augmented EndMT changes in vivo and increased TGF-β/Smad2/3 signaling. We found that activation of EC FGFR1 signaling repressed EndMT. These studies establish the importance of EC FGFR signaling in the pathogenesis of hypoxia-induced PH and suggest the possibility of future FGF pathway–based therapeutics aimed at reducing the severity of PH in hypoxia-challenged patients.

Results

FGFR1 and FGFR2 inactivation in ECs worsens in vivo hypoxia-PH. To determine the effect of hypoxia on *Fgf2* expression, 6-week-old mice were challenged with hypoxia (10% FiO₂) for 2 weeks. Quantitative real-time PCR (qRT-PCR) analysis of whole lungs from mice exposed to 2 weeks of hypoxia or normoxia showed increased expression of *Fgf2* (Figure 1A). To ascertain the requirements for FGF signaling in ECs in response to hypoxia, 6-week-old *Flk1*(*Vegfr2/Kdr*)^{Cre}; *Fgfr1*$^{fl/fl}$; *Fgfr2*$^{fl/fl}$ (FLK1-DCKO) and *Flk1*^{Cre} or *Fgfr1*$^{fl/fl}$; *Fgfr2*$^{fl/fl}$ (control) mice were challenged with hypoxia for 2 weeks. Cardiac catheterization was used to measure RV pressure (RVp) as a surrogate for pulmonary arterial pressure. Compared with control mice in normoxia, littermates in hypoxia demonstrated significant increases in RVp (Figure 1B) and the RV to left ventricle plus septum weight ratio (Figure 1, C and D), consistent with development of PH and RV hypertrophy, respectively. Hypoxia-exposed FLK1-DCKO mice (hFLK1-DCKO) showed further elevation in RVp (by 24.4%, *P* < 0.05) (Figure 1B) and an increased RV to left ventricle plus septum weight ratio as compared with controls (hControl; Figure 1, C and D), demonstrating worsening PH in the absence of EC FGF signaling. *Flk1*^{Cre} (a knock-in mutation at the *Vegfr2/Kdr* locus) and wild-type mice under normoxic conditions did not show any difference in RVp (Supplemental Figure 1A; supplemental material available online with this article; https://doi.org/10.1172/JCI141467DS1). Hypoxia-challenged *Flk1*^{Cre} and wild-type mice also did not show any difference in RVp (Supplemental Figure 1B).

The echocardiographic imaging marker, pulmonary artery acceleration time (PAAT), has been validated for detection of pulmonary vascular disease and PH in mice (43). Comparison of echocardiographic and cardiac catheterization measures showed a strong correlation of PAAT (Figure 1E) and PAAT normalized to RV ejection time (PAAT/RVET) (Figure 1F) with RVp
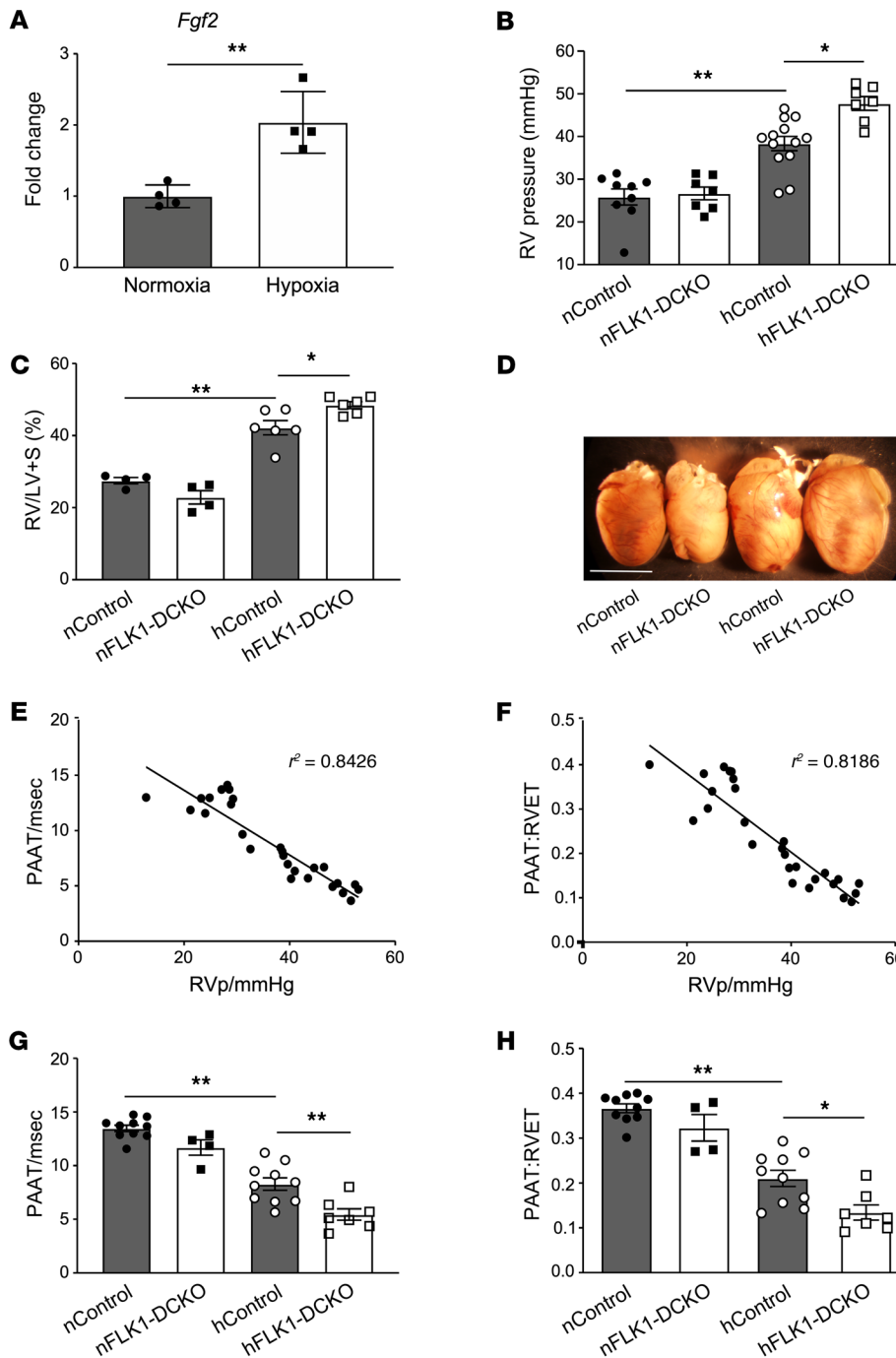
Figure 1. Increased severity of pulmonary hypertension in mice lacking endothelial FGFR1 and FGFR2. Pulmonary hypertension assessment after 2 weeks of hypoxia exposure (white column) compared with normoxia controls (gray column). (**A**) Quantitative RT-PCR showing *Fgf2* expression in whole lungs from wild-type mice, *n* = 4. Statistical significance was determined by 2-tailed, unpaired Student's *t* test. (**B**) RV pressures determined by cardiac catheterization of hypoxia-challenged control (*Flk1^Cre* or *Fgfr1^fl/fl*; *Fgfr2^fl/fl*) and FLK1-DCKO mice compared with littermates in normoxia, *n* = 7–13. (**C**) RV to left ventricular plus septal (RV/LV+S) weight comparison between hypoxia-exposed control and FLK1-DCKO mice compared with littermates in normoxia, *n* = 4–6. (**D**) Representative specimens of whole hearts. Scale bar: 10 mm. (**E**) Correlation plot of right heart catheterization–derived pulmonary hemodynamics and pulmonary artery acceleration time (PAAT) from all mice (normoxia and hypoxia), *n* = 26. (**F**) Correlation plot of right heart catheterization–derived pulmonary hemodynamics and PAAT/RV ejection time ratio (PAAT/RVET), *n* = 26. (**G** and **H**) Comparison of PAAT (**G**) and PAAT/RVET (**H**) in hypoxia-challenged FLK1-DCKO and control mice, *n* = 4–10. Statistical significance was determined by 2-way ANOVA with Holm-Šídák multiple comparison test. All data are shown as the mean ± SEM. *$P <$ 0.05, **$P <$ 0.01. Closed circles, control mice in normoxia (nControl); open circles, control mice in hypoxia (hControl); closed squares, FLK1-DCKO mice in normoxia (nFLK1-DCKO); open squares, FLK1-DCKO mice in hypoxia (hFLK1-DCKO).

in hypoxia-challenged mice. PAAT was decreased in control hypoxia-exposed mice compared with normoxia controls and FLK1-DCKO mice showed a further decrease when compared with control mice in hypoxia (Figure 1G). The PAAT/RVET ratio showed a significant decrease in hypoxia compared with normoxia-exposed mice and FLK1-DCKO mice showed a further decrease in these measures after 2 weeks in hypoxia (Figure 1H). Therefore, loss of EC FGFR signaling is sufficient to increase hypoxia-induced PH.

Histologic analyses of the pulmonary arteries showed increased medial thickening in control mice in hypoxia as compared with littermates in normoxia (Figure 2A). Compared with

control mice in normoxia, littermates in hypoxia demonstrated significant increase in medial areas of both smaller caliber, distal vessels (20–50 μm, Figure 2B) and larger caliber, proximal vessels (50–100 μm, Figure 2C). FLK1-DCKO mice showed further increases in the vascular medial area as compared with controls (Figure 2, A–C), demonstrating more severe pulmonary vascular remodeling. To assess neomuscularization, lung tissue sections were coimmunostained with antibodies against PECAM1 and αSMA to identify ECs and VSM, respectively. Hypoxia reduced the proportion of nonmuscularized and partially muscularized vessels and increased the proportion of fully muscularized vessels as compared with normoxia controls
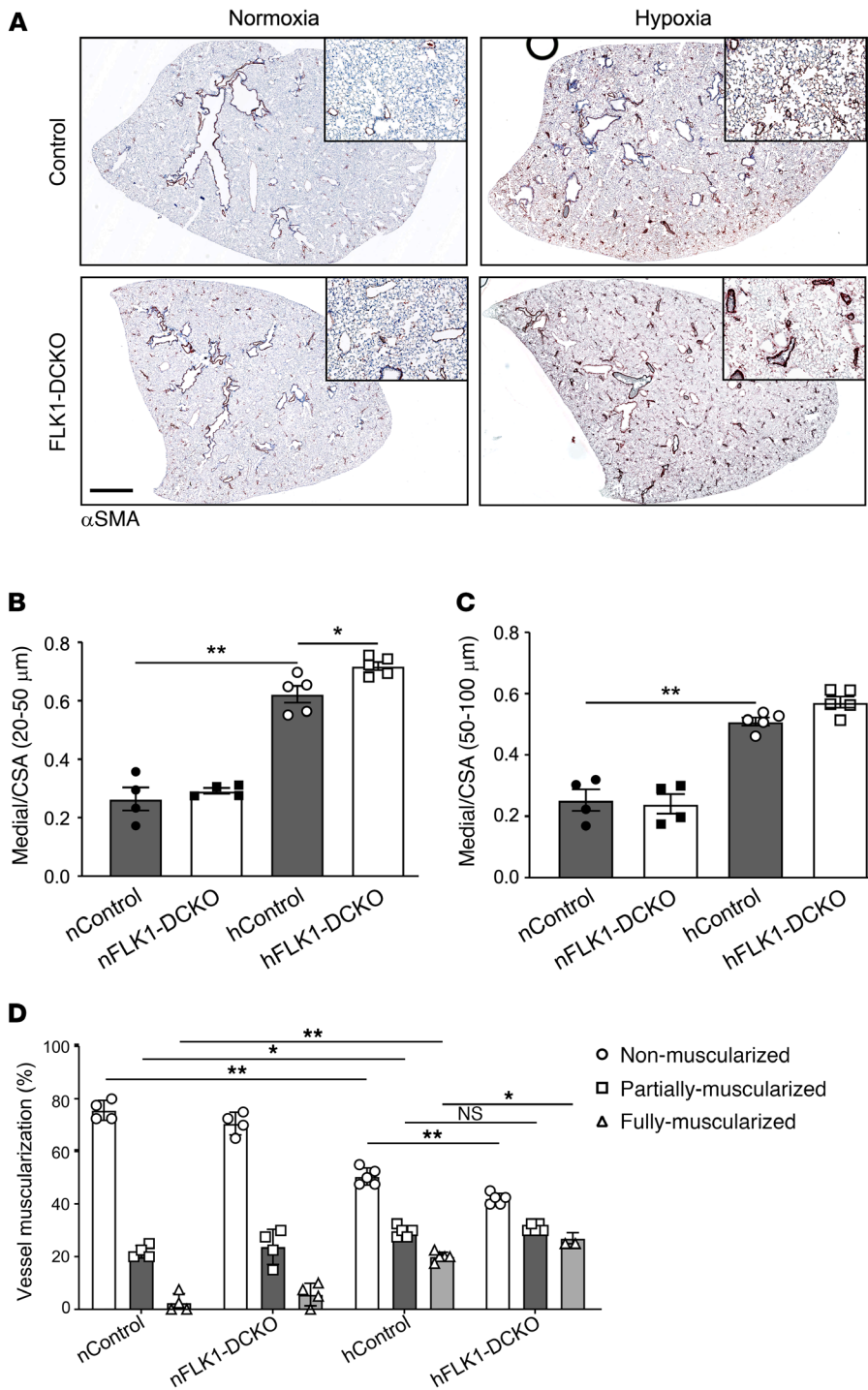
Figure 2. Histologic analysis of the pulmonary vasculature in mice lacking endothelial FGFR1 and FGFR2. (**A**) Smooth muscle actin (αSMA) immunostaining of representative lungs from control and FLK1-DCKO mice in normoxia and hypoxia. Scale bars: 1 mm and 50 μm (insets). (**B** and **C**) Vessel wall thickening as assessed by medial cross-sectional area normalized to total vessel cross-sectional area (medial/CSA) for (**B**) distal vessels (20–50 μm) and (**C**) proximal vessels (50–100 μm), $n = 4–5$. (**D**) Quantification of the percentage of muscularized vessels compared with total number of vessels, in normoxia- and hypoxia-exposed control and FLK1-DCKO mice, $n = 4–5$. Statistical significance was determined by 2-way ANOVA with Holm-Šídák multiple comparison test. All data are shown as the mean ± SEM. $*P < 0.05$, $**P < 0.01$. Closed circles, control mice in normoxia (nControl); open circles, control mice in hypoxia (hControl); closed squares, FLK1-DCKO mice in normoxia (nFLK1-DCKO); open squares, FLK1-DCKO mice in hypoxia (hFLK1-DCKO).

(Figure 2D). FLK1-DCKO mice showed a further increase in the proportion of fully muscularized vessels when compared with control littermates in hypoxia (Figure 2D). Thus, loss of EC FGFR signaling augments vascular changes associated with hypoxia-induced PH.

To rule out potential developmental effects due to constitutive loss of EC *Fgfr1* and *Fgfr2* and heterozygosity of *Vegfr2* (*Flk1^Cre^*) on PH pathology, the conditional *Cdh5*-CreERT2 transgenic allele was used to inactivate *Fgfr1* and *Fgfr2* and activate the *ROSA^tdTomato^* lineage reporter in ECs of juvenile mice. Three-week-old *Cdh5*-CreERT2; *Fgfr1^fl/fl^*; *Fgfr2^fl/fl^*; *ROSA^tdTomato^* (Cdh5-DCKO) and control *Fgfr1^fl/fl^*; *Fgfr2^fl/fl^* (control) mice were treated with tamoxifen from 3–4 weeks of age (Figure 3A). Lineage analysis showed colabeling of PECAM1 and tdTomato fluorescence, confirming EC targeting by tamoxifen-treated *Cdh5*-CreERT2; *ROSA^tdTomato^* mice (Figure 3B). Transcriptional analysis of pulmonary ECs isolated from mouse lungs using flow cytometry showed that *Fgfr1* (Figure 3C) and *Fgfr2* (Figure 3D) expression was significantly decreased. Cdh5-DCKO mice were challenged with hypoxia for 2 weeks, followed by cardiac catheterization to measure RVp. Compared with control mice exposed to hypoxia, Cdh5-DCKO mice demonstrated significant increases in RVp (by 13.2%, $P < 0.05$) (Figure 3E). These results show that loss of EC FGFR1 and FGFR2 beginning at 3 weeks of age worsens hypoxia-induced PH, similar to FLK1-DCKO mice.

FGFR1 activation in ECs prevents hypoxia-induced PH. Because loss of EC *Fgfr1* and *Fgfr2* leads to VSM thickening in response to hypoxia, we hypothesized that expression of a constitutively active FGFR1 (caFGFR1) in ECs would protect against maladaptive vessel muscularization in hypoxia-induced PH. To investigate the cell-autonomous function of FGF signaling in ECs, we utilized the Tie2-Cre transgenic allele to target the doxycycline-inducible TET-on Cre-regulatable *ROSA^rtTA^* allele, and a chimeric constitutively active *Fgfr1* transgenic allele (TRE-caFgfr1) in ECs. We generated Tie2-Cre; *ROSA^rtTA^*; TRE-caFgfr1 (caFGFR1) triple-transgenic mice (Figure 4A) to conditionally activate EC FGFR signaling. Doxycycline treatment, starting at 4 weeks of age for 2 weeks, increased *caFGFR1* expression in lungs of caFGFR1 compared with control mice (Fig-
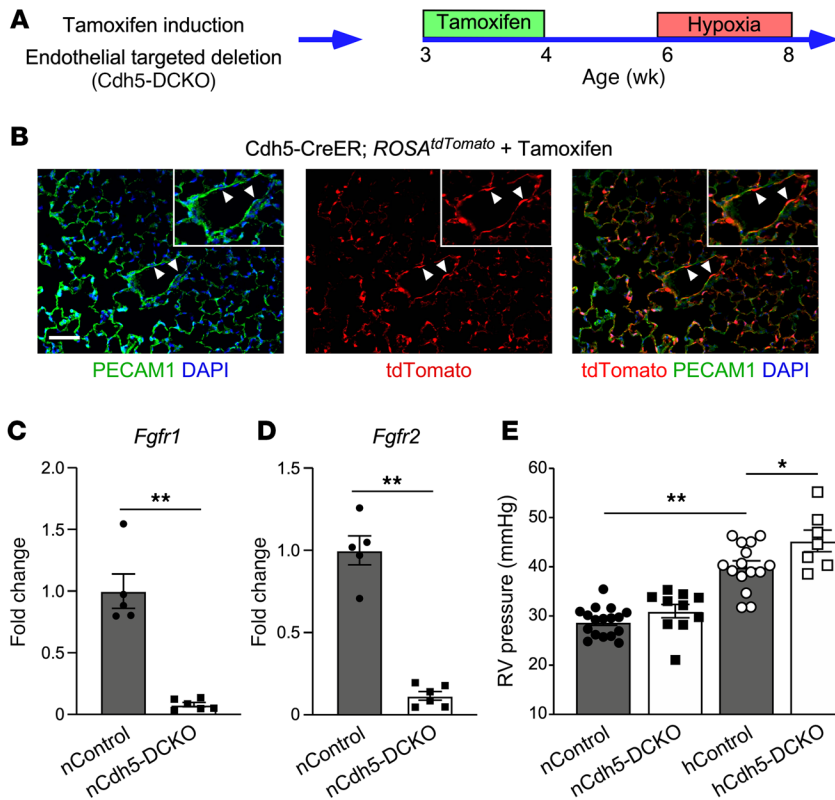
Figure 3. Effects of conditional deletion of *Fgfr1* and *Fgfr2* in endothelial cells on hypoxia-induced pulmonary hypertension. (**A**) Experimental strategy for tamoxifen-induced *Cdh5*-targeted deletion of *Fgfr1* and *Fgfr2* in endothelial cells (ECs). (**B**) Tamoxifen-induced *Cdh5*-targeted tdTomato (red) expression in ECs (PECAM1, green, arrowheads). Scale bars: 25 μm and 20 μm (insets). (**C** and **D**) Quantitative RT-PCR showing reduction of *Fgfr1* and *Fgfr2* expression in pulmonary ECs of tamoxifen-treated (Cdh5-DCKO) mice compared with control littermates, *n* = 5–6. Statistical significance was determined by 2-tailed, unpaired Student's *t* test. (**E**) RV pressures determined by cardiac catheterization of hypoxia-challenged control and Cdh5-DCKO mice, *n* = 7–17. Statistical significance was determined by 2-way ANOVA with Holm-Šídák multiple comparison test. All data are shown as the mean ± SEM. *$P < 0.01$, **$P < 0.05$. Closed circles, control mice in normoxia (nControl); open circles, control mice in hypoxia (hControl); closed squares, Cdh5-DCKO mice in normoxia (nCdh5-DCKO); open squares, Cdh5-DCKO mice in hypoxia (hCdh5-DCKO).

ure 4B). In prior studies, induction of caFGFR1 in ECs for 1 month did not have any apparent adverse effects (44).

Four-week-old caFGFR1 and control mice were placed on doxycycline chow. Starting at 6 weeks of age, mice were challenged with hypoxia for 2 weeks, followed by cardiac catheterization to measure RVp. In response to hypoxia, control mice demonstrated significant increases in RVp (Figure 4C) and the RV to left ventricle plus septum weight ratio (Figure 4, D and E), consistent with development of PH. At baseline, caFGFR1 mice compared with control mice in normoxia showed no difference in RVp (Figure 4C) and the RV to left ventricle plus septum weight ratio (Figure 4D). However, in response to hypoxia, caFGFR1 mice showed similar RVp and RV to left ventricle plus septum weight ratio compared to normoxia mice, and significantly lowered RVp (by 23.7%, *P* < 0.05) and RV to left ventricle plus septum weight ratio compared with hypoxia-exposed control mice (Figure 4, C and D). Therefore, activation of EC FGFR1 signaling is sufficient to prevent hypoxia-induced PH.

Effects of hypoxia on the pulmonary vasculature of caFGFR1 mice were consistent with resistance to the development of PH (Figure 5A). In normoxia, caFGFR1 mice and control mice showed no difference in the medial area of both smaller caliber distal vessels (20–50 μm, Figure 5B) and larger caliber proximal vessels (50–100 μm, Figure 5C). In response to hypoxia, control mice demonstrated significant increases in the medial area of both large and small caliber vessels (Figure 5, B and C). However, in response to hypoxia, caFGFR1 mice showed similar medial areas of small caliber vessels to those of mice in normoxia and no difference in the medial area of smaller caliber vessels in caFGFR1 mice in hypoxia versus normoxia (Figure 5B). The medial area of large

caliber vessels was modestly increased (1.6-fold) when comparing caFGFR1 mice in hypoxia versus normoxia; however, the medial area of large caliber vessels was still much reduced compared with control mice in hypoxia (4.0-fold) (Figure 5C).

To assess neomuscularization, lung tissue sections were coimmunostained for PECAM1 and αSMA to identify ECs and VSM cells, respectively. In normoxia, caFGFR1 and control mice showed no difference in the proportions of nonmuscularized, partially muscularized, and fully muscularized vessels (Figure 5D). In response to hypoxia, control mice demonstrated a significant reduction in the proportion of nonmuscularized and partially muscularized vessels, and an increase in the proportion of fully muscularized vessels (Figure 5D). However, in response to hypoxia, caFGFR1 mice showed similar proportions of vessel muscularization to those of mice in normoxia, and a significantly lower proportion of fully muscularized vessels compared with hypoxia-exposed control mice (Figure 5D). These results demonstrate that EC FGFR1 activity reduces histologic changes in the vasculature associated with hypoxia-induced PH.

FGF signaling reduces hypoxia-induced EndMT. Reprograming of ECs to VSM (Figure 6A), a process known as EndMT, underlies several disease pathologies (18–20). To evaluate the effect of hypoxia on EndMT, Tie2-Cre; *ROSA^{tdTomato}* EC-lineage reporter mice were exposed to hypoxia (Figure 6B). After 2 weeks in hypoxia, VSM cells in the tunica media layer were found to express the tdTomato EC-lineage tag (Figure 6B), indicating an EndMT response to hypoxic conditions. Normoxia control mice showed no tdTomato fluorescence in αSMA-positive cells. Hypoxia-exposed control mice were also coimmunostained for PECAM1 and αSMA to demonstrate EndMT (Figure 6C). VSM cells in the medial
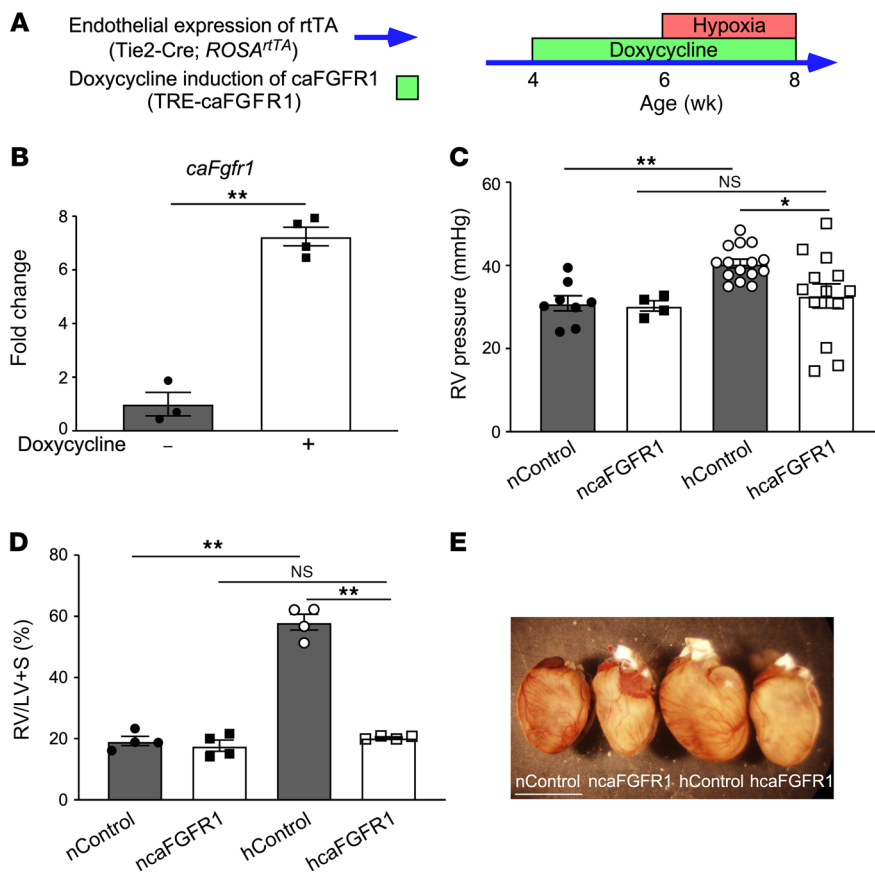
Figure 4. Effects of cell-autonomous activation of FGFR1 in endothelial cells on the development of hypoxia-induced pulmonary hypertension. (**A**) Experimental strategy for expressing the tetracycline-inducible constitutively active FGFR1 (caFGFR1) in endothelial cells (ECs). Tie2-Cre; *ROSA^{rtTA}* results in reverse tetracycline-controlled transactivator (rtTA) expression in ECs (blue arrow), and in the presence of doxycycline (green box), TRE-caFGFR1 expression is induced in ECs (TIE2-caFGFR1 = Tie2-Cre; *ROSA^{rtTA}*; TRE-caFgfr1). (**B**) Quantitative RT-PCR showing induction of *caFGFR1* expression in lungs of doxycycline-treated compared with untreated mice, *n* = 3–4. Statistical significance was determined by 2-tailed, unpaired Student's *t* test. (**C**) RV pressures determined by cardiac catheterization of hypoxia-challenged control and caFGFR1 mice, *n* = 4–15. (**D**) Right ventricular to left ventricular plus septal (RV/LV+S) weight comparison between control and caFGFR1 mice, *n* = 4. (**E**) Representative whole hearts. Scale bar: 10 mm. Statistical significance was determined by 2-way ANOVA with Holm-Šídák multiple comparison test. All data are shown as the mean ± SEM. NS, not significant. *$P < 0.05$, **$P < 0.01$. caFGFR1 = Tie2-Cre; *ROSA^{rtTA}*; TRE-caFgfr1. Closed circles, control mice in normoxia (nControl); open circles, control mice in hypoxia (hControl); closed squares, TIE2-caFGFR1 mice in normoxia (ncaFGFR1); open squares, TIE2-caFGFR1 mice in hypoxia (hcaFGFR1).

layer expressed the endothelial marker PECAM1 (Figure 6C), further supporting an EndMT response to hypoxic conditions.

To determine whether loss of FGFR1 and FGFR2 signaling in EC affects EndMT, *Fgfr1^{fl/fl}*; *Fgfr2^{fl/fl}* control and *Flk1^{Cre}*; *Fgfr1^{fl/fl}*; *Fgfr2^{fl/fl}*; *ROSA^{tdTomato}* (FLK1-DCKO/Tomato) mice were examined. In normoxia, control and FLK1-DCKO/Tomato mice did not show any difference in the proportion of VSM cells with the tdTomato EC-lineage tag (Figure 7A). In mice exposed to hypoxia, control mice showed a significant increase in the percentage of EC lineage–tagged VSM cells compared with normoxia, and hypoxia-exposed FLK1-DCKO/Tomato mice demonstrated a further increase in the percentage of VSM cells derived from the EC lineage (Figure 7A). To determine the effects of activation of FGFR1 signaling on EndMT, we used the caFGFR1 mouse model. Four-week-old caFGFR1 and control mice were placed on doxycycline chow. Starting at 6 weeks of age, mice were challenged with hypoxia for 2 weeks. Under normoxic conditions, caFGFR1 and control mice did not show any difference in the proportion of VSM cells derived from the EC lineage (Figure 7B). Relative to mice in normoxia, control mice exposed to hypoxia showed a significant increase in the percentage of VSM cells derived from the EC lineage. Compared with control mice in hypoxia, caFGFR1 mice in hypoxia showed a significant reduction in EndMT (Figure 7B), indicating that activation of FGFR1 in ECs inhibits EndMT.

FLK1-DCKO/Tomato and *Fgfr1^{fl/fl}*; *Fgfr2^{fl/fl}* control mice were also coimmunostained for PECAM1 and αSMA to demonstrate EndMT. In normoxia, FLK1-DCKO mice did not show any

difference in the proportion of VSM cells expressing PECAM1 (Figure 7C). In mice exposed to hypoxia, control mice showed a significant increase in the percentage of PECAM1-expressing VSM cells compared with normoxia, and hypoxia-exposed FLK1-DCKO demonstrated a further increase in the percentage of VSM cells expressing the EC marker, PECAM1 (Figure 7C). Under normoxic conditions, caFGFR1 and control mice did not show any difference in the proportion of VSM cells expressing PECAM1 (Figure 7D). Control mice exposed to hypoxia showed a significant increase in the percentage of VSM cells expressing PECAM1, compared with mice in normoxia. Relative to control mice in hypoxia, caFGFR1 mice in hypoxia showed a significant reduction in EndMT (Figure 7D), further demonstrating that EC FGFR1 activation inhibits EndMT.

FGF signaling inhibits the TGF-β pathway response to hypoxia in vivo. TGF-β signaling regulates EndMT in Group 1 PAH and atherosclerosis (20, 45). To evaluate the effect of EC *Fgfr1* and *Fgfr2* deletion on TGF-β signaling, qRT-PCR analysis was performed on RNA from whole lungs of FLK1-DCKO and control mice exposed to 2 weeks of hypoxia or normoxia. In normoxia, FLK1-DCKO mice did not show any differences in expression of TGF-β pathway components compared to controls (Figure 8A). FLK1-DCKO mice in hypoxia demonstrated increased expression of *Tgfbr2*, *Snai1*, *Snai2*, *Twist1*, and *Acta2* and decreased expression of *Pecam1* (Figure 8A). *Tgfb1* and *Tgfb2* ligand expression was decreased in hypoxia-exposed FLK1-DCKO mice compared with controls (Supplemental Figure 2). FLK1-DCKO mice
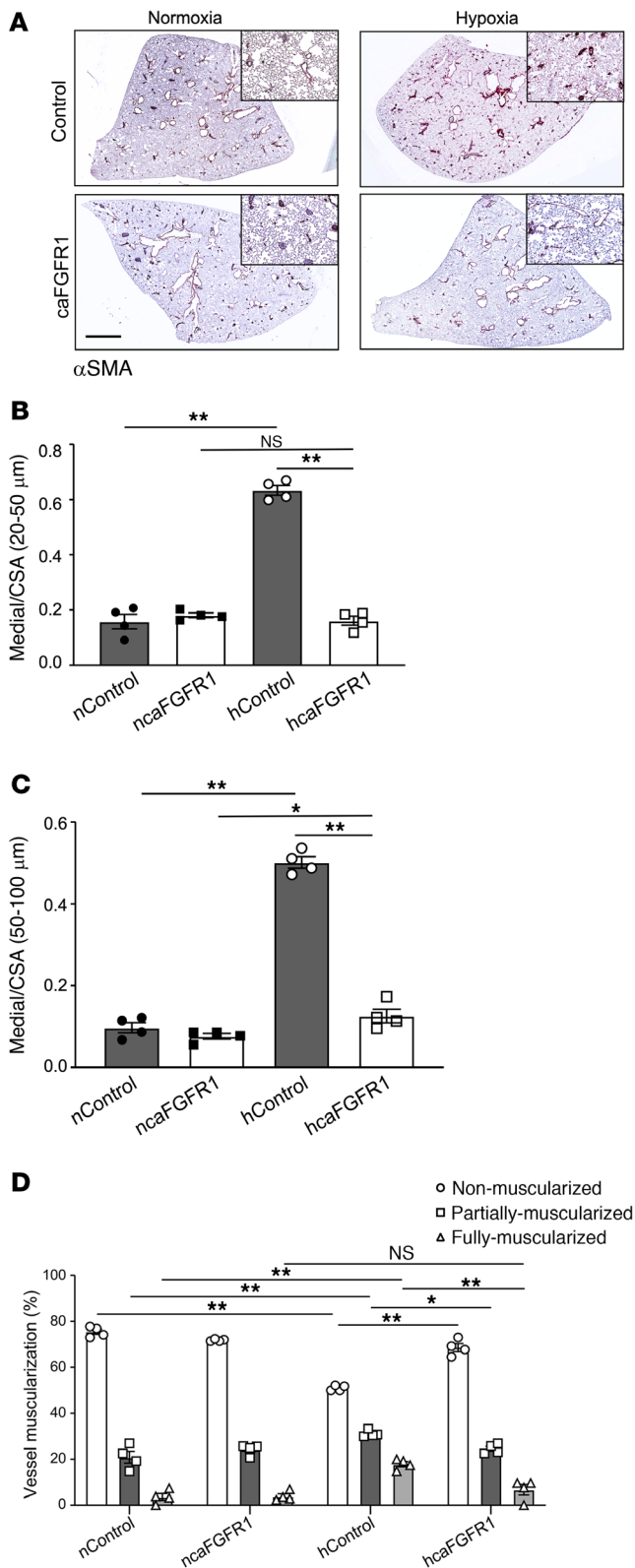
Figure 5. Constitutively active FGFR1 reduces the pulmonary vascular response to hypoxia. (**A**) Smooth muscle actin (αSMA) immunostaining of representative lungs from control and caFGFR1 mice in normoxia and hypoxia. Scale bars: 1 mm and 50 μm (insets). (**B** and **C**) Vessel wall thickening as assessed by medial cross-sectional area normalized to total vessel cross-sectional area (medial/CSA) for (**B**) distal vessels (20–50 μm) and (**C**) proximal vessels (50–100 μm), n = 4. (**D**) Quantification of the percentage of muscularized vessels compared with total number of vessels, in normoxia- and hypoxia-exposed control and caFGFR1 mice, n = 4. Statistical significance was determined by 2-way ANOVA with Holm-Šídák multiple comparison test. All data are shown as the mean ± SEM. NS, not significant. *$P < 0.05$, **$P < 0.01$. caFGFR1 was induced as shown in Figure 4A. Closed circles, control mice in normoxia (nControl); open circles, control mice in hypoxia (hControl); closed squares, TIE2-caFGFR1 mice in normoxia (ncaFGFR1); open squares, caFGFR1 mice in hypoxia (hcaFGFR1).

of caFGFR1 and control mice that were exposed to 2 weeks of hypoxia or normoxia. In normoxia, there was no difference in the expression of TGF-β pathway components in caFGFR1 and control mice (Figure 8B). In hypoxia, control mice showed increased expression of *Tgfbr2*, *Snai1*, *Snai2*, and *Fgf2*, while *Twist1*, *Pecam1*, and *Acta2* expression was not changed. However, in hypoxia, compared with controls, caFGFR1 mice showed lower levels of *Tgfbr2*, *Snai1*, *Snai2*, *Twist1*, and *Fgf2*, and similar levels of *Pecam1* and *Acta2*. *Tgfb1* and *Tgfb2* ligand expression was decreased in hypoxia-exposed caFGFR1 mice compared with controls (Supplemental Figure 2). Notably, caFGFR1 mice in normoxia did not show any differences in expression of *Fgf2*, whereas control mice in hypoxia showed significantly higher levels of *Fgf2* (Figure 8B).

To directly assess TGF-β signaling in vivo, we immunostained lung tissue for p-Smad2/3 in both mouse models. In control lungs, hypoxia exposure increased p-Smad2/3 compared with normoxia (Figure 9). Under hypoxic conditions, FLK1-DCKO mice showed a further increase in the percentage of p-Smad2/3–expressing ECs compared with control mice (Figure 9A) and caFGFR1 mice showed less p-Smad2/3 expression in ECs (Figure 9B). These results demonstrate that FGF signaling suppresses TGF-β signaling and EndMT in response to hypoxia.

FGF inhibition promotes EndMT in vitro. To directly assess the effects of FGF inhibition on EndMT, human pulmonary artery ECs (HPAECs) were cultured in hypoxia (5% O$_2$) for 48 hours (Figure 10A) or 14 days (Figure 10B), and then assayed for changes in RNA expression of TGF-β pathway components and markers of EndMT. After 48 hours, treatment with the FGF inhibitor BGJ398 (infigratinib) under normoxic conditions increased *Tgfb2* 21-fold, increased *Acta2* and *Fgf2*, and decreased *Cdh5*, but did not change the expression of the transcription factors *Snai2* and *Twist1* and the mesenchymal marker *Vim*. FGF inhibition under hypoxic conditions increased *Tgfb2* (40-fold), *Snai2*, and *Twist1*, and decreased *Cdh5*. Expression of *Acta2* and *Fgf2* trended toward an increase.

HPAECs were then cultured for 14 days to evaluate the effects of chronic hypoxia and FGF inhibition on EndMT in vitro (Figure 10B). In normoxia, FGF inhibition with BGJ398 did not exert any significant effects on expression of *Tgfb2*, *Snai2*, *Twist1*, *Cdh5*, or *Vim*, whereas expression of *Fgf2* was increased and *Acta2* trended toward an increase. However, when cultured in hypoxia, BGJ398-treated HPAECs demonstrated increased expression of

in normoxia also did not show any differences in the expression of *Fgf2* (Figure 8A). In hypoxia, control mice demonstrated increased *Fgf2* and hypoxia-exposed FLK1-DCKO mice showed a further increase in *Fgf2* expression.

To evaluate the effect of activation of FGFR1 signaling in ECs, qRT-PCR analysis was performed on RNA from whole lungs
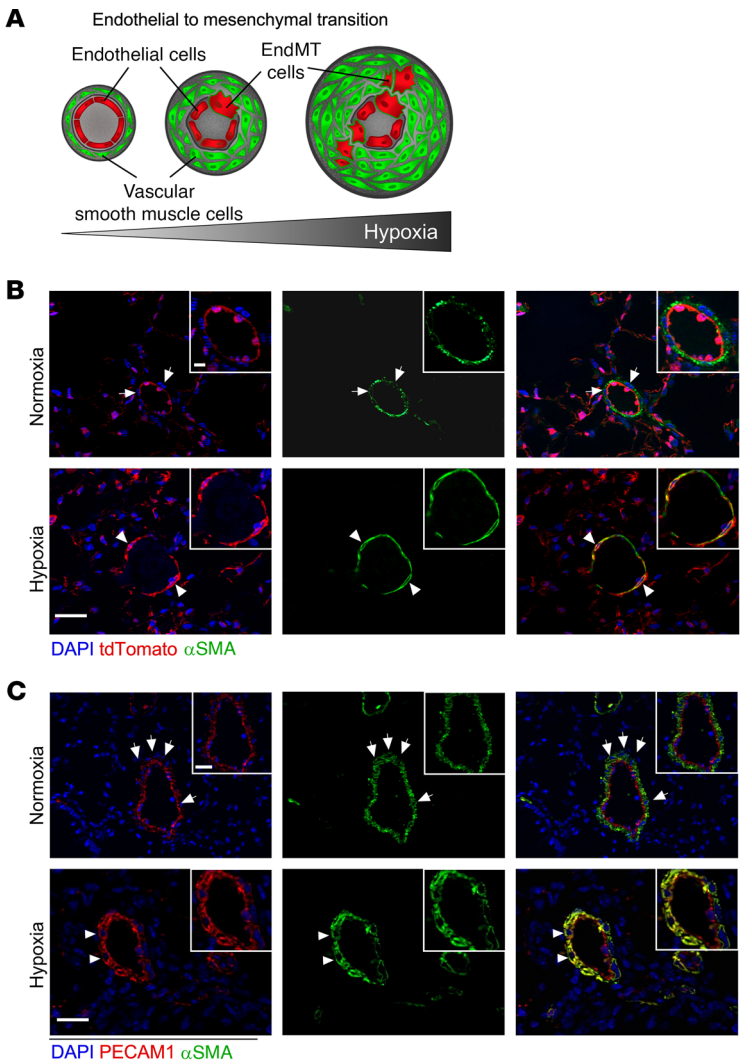
Figure 6. FGFR signaling regulates endothelial-mesenchymal transition in hypoxia-induced pulmonary hypertension. (**A**) Illustration depicting the process of endothelial-mesenchymal transition (EndMT). (**B**) Lineage tracing visualized by immunostaining smooth muscle cells (αSMA, green) expressing endothelial origins (Tie2-Cre; *ROSA^tdTomato*, red) after 2 weeks of hypoxia. Scale bars: 25 μm and 15 μm (insets). Inset, higher magnification image illustrating overlay of αSMA (green) and endothelial lineage tdTomato (red). (**C**) Lineage tracing visualized by immunostaining smooth muscle cells (αSMA, green) expressing endothelial origins (PECAM1, red) after 2 weeks of hypoxia. Scale bars: 25 μm and 15 μm (insets). Inset, higher magnification image illustrating overlay of αSMA (green) and PECAM1 (red). Arrows, non–endothelial origin smooth muscle cells; arrowheads, endothelium-originated smooth muscle cells.

Tgfb2, *Twist1*, and *Acta2*, a trend toward increased expression of *Snai2* and *Fgf2*, and decreased expression of *Cdh5* (Figure 10B). Notably, chronic hypoxia increased expression of *Fgf2* and downstream transcriptional targets of FGF signaling, ETS transcription variant 4 and 5 (*Etv4* and *Etv5*), and dual-specificity phosphatase 6 (*Dusp6*) (Figure 10, B and C). As expected, expression of *Etv4* was decreased with FGFR inhibition (Supplemental Figure 4).

Compared with normoxia, exposure to 5% oxygen for 14 days did not induce expression of αSMA in HPAECs (Figure 11A). However, HPAECs exposed to 5% oxygen for 14 days and treated with BGJ398 formed colonies of αSMA-expressing cells, demon-

strating EndMT in vitro (Figure 11A). Quantitative analyses showed an increased number of colonies of αSMA-positive cells per well in BGJ398-treated hypoxia-exposed HPAECs, and no colonies in untreated or normoxia-cultured wells (Figure 11B). Western blot analysis showed no difference in Smad2/3 phosphorylation or ACTA2 expression in normoxia. BGJ398 treatment increased Smad2/3 phosphorylation and αSMA expression in hypoxia-exposed HPAECs (Figure 11, C and D). These data demonstrate that, in response to hypoxia, EndMT activity and TGF-β signaling are increased when FGF signaling is inhibited (Figure 11, D and E).

EndMT observed in patients with CPFE and PH. Group 3 PH can be caused by hypoxia resulting from lung disorders such as COPD, BPD, or CPFE (1, 2). To evaluate the presence of molecules known to mediate EndMT in CPFE, we assessed histological sections of lungs from patients with CPFE in comparison with normal lung tissue. Patients with CPFE had average mean pulmonary artery pressure of 31 mmHg (Supplemental Table 1), above the diagnostic criteria of 25 mmHg for PH. To assess FGF and TGF-β signaling, we examined expression of ETV5 and p-Smad2/3, respectively. Compared with controls, lung tissue sections from patients with CPFE showed decreased immunostaining for ETV5 (Figure 12A). In normal lung tissue, an average of 95% of CDH5-positive ECs were positive for ETV5, compared with 73% in CPFE lung tissue (Figure 12C). Immunostaining for p-Smad2/3 showed increased expression in CPFE lung tissue compared with normal lung tissue (Figure 12B). In normal lung tissue, an average of 50% of CDH5-positive ECs were positive for p-Smad2/3, compared with 64% of CDH5-positive ECs that were positive for p-Smad2/3 in CPFE lung tissue (Figure 12D). These data correlate pulmonary pathologies such as CPFE that contribute to Group 3 PH with reduced FGF signaling and increased TGF-β signaling, similarly to experimental conditions that promote EndMT such as chronic hypoxia.

Discussion

The results of this study support a role for EC FGFR signaling as a modulator of the EndMT response in the pathogenesis of hypoxia-induced PH. We showed that in response to chronic hypoxia, (a) loss of EC FGFR1 and FGFR2 signaling increased PH, (b) activation of FGFR1 in ECs prevented PH, (c) EC FGFR signaling attenuated the TGF-β signaling pathway, and (d) FGFR signaling was reduced and TGF-β signaling was activated in lung tissue from patients with CPFE. Taken together, these results establish a link between hypoxia, the loss of protective EC FGFR signaling input, and the induction of EndMT, which ultimately plays an important role in the pathogenesis of hypoxia-induced PH.

FGFR1 is robustly expressed, while FGFR2 and -3 are expressed at lower levels in normal ECs (40, 41, 46–48). Under homeostatic conditions, inactivation of EC *Fgfr1* and *Fgfr2* did not cause any overt developmental or homeostatic defects. However, several studies showed that loss or inhibition of these
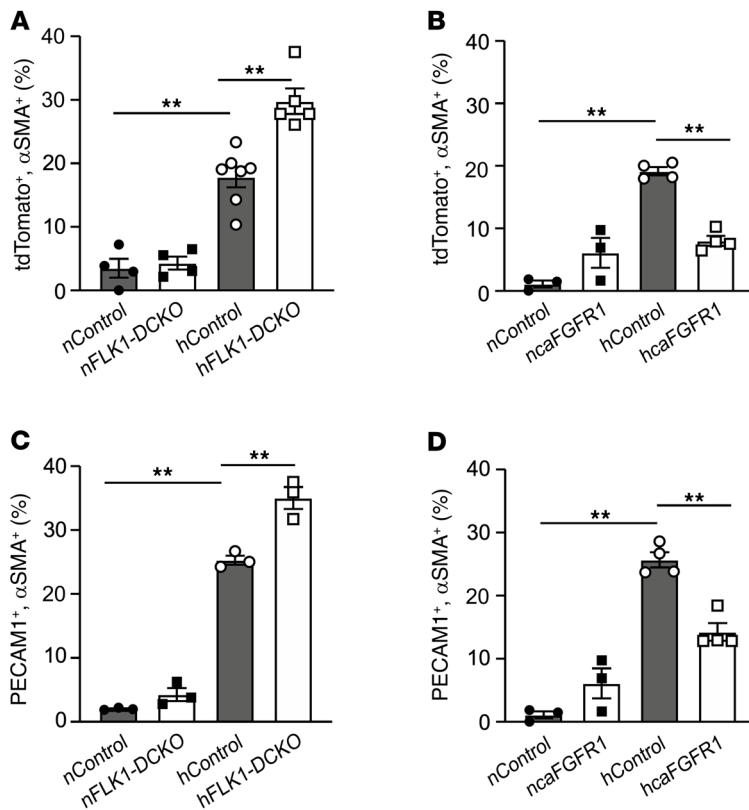
Figure 7. FGFR signaling regulates endothelial-mesenchymal transition in hypoxia-induced pulmonary hypertension. Quantification of EndMT shown as a percentage of tdTomato+αSMA+ double-positive cells in relation to the total number of αSMA+ cells in (**A**) FLK1-DCKO mice (*n* = 4–6) and (**B**) caFGFR1 mice (*n* = 4–7). Quantification of EndMT shown as a percentage of PECAM1+αSMA+ double-positive cells in relation to the total number of αSMA+ cells in (**C**) FLK1-DCKO mice (*n* = 3) and (**D**) caFGFR1 mice (*n* = 3–4). Statistical significance was determined by 2-way ANOVA with Holm-Šídák multiple comparison test. All data are shown as the mean ± SEM. **P < 0.01. Closed circles, control mice in normoxia (nControl); open circles, control mice in hypoxia (hControl); closed squares, *Flk1^Cre^*; *Fgfr1^fl/fl^*; *Fgfr2^fl/fl^* mice in normoxia (nFLK1-DCKO) or caFGFR1 mice in normoxia (ncaFGFR1); open squares, *Flk1^Cre^*; *Fgfr1^fl/fl^*; *Fgfr2^fl/fl^* mice in hypoxia (hFLK1-DCKO) or caFGFR1 mice in hypoxia (hcaFGFR1).

receptors in ECs leads to defective injury responses (39–41, 49). Based on these observations, we hypothesized that EC FGFR signaling would be protective against the adaptive vascular response to hypoxia. To test this, two models were used to inactivate floxed alleles of *Fgfr1* and *Fgfr2* in ECs: constitutive targeting with *Flk1^Cre^* (FLK1-DCKO) and inducible targeting with *Cdh5*-CreER (Cdh5-DCKO).

Group 3 PH can be modeled by placing mice in normobaric chambers at 10% effective oxygen, which results in a reliable increase in RVp by at least 10 mmHg, RV hypertrophy, and pulmonary vascular remodeling (50). Additionally, after exposing 6-week-old mice to 10 days of hypoxia, pulmonary artery vessel wall thickness was increased (51). To assess the in vivo role of FGFR signaling in the development of PH, we investigated the effect of loss of FGFR signaling in mice with experimental PH induced by hypoxia. Under normoxic conditions, inactivation of EC FGFR1/2 signaling with *Flk1^Cre^* (FLK1-DCKO) did not result in any identifiable physiologic or histologic phenotypes, consistent with previous findings that EC FGFR signaling is not

required under homeostatic conditions (39, 40). By contrast, under hypoxic conditions, FLK1-DCKO mice demonstrated increased vessel wall thickness and neovascularization when compared with their littermate controls. These results show that loss of EC FGFR signaling promotes changes that are associated with hypoxia-induced PH.

The *Flk1^Cre^* mouse is heterozygous for *Vegfr2* (*Kdr*). Haploinsufficiency of *Vegfr2* suppresses tumor-induced angiogenesis (52) and leads to increased infarct size in a myocardial ischemia-reperfusion injury model (53). Additionally, pharmacological inhibition of VEGFR is an important regulator of PH (54), and mice treated with the VEGFR inhibitor SU5416 exhibited PH changes in response to hypoxia (55, 56). Furthermore, mice heterozygous for *Vegfr2* show reduced pathological angiogenesis (57, 58). It was therefore important to assess the effects of *Vegfr2* haploinsufficiency on hypoxia-induced PH. Although VEGFR2 activity is vital to vascular development (59), we did not observe any identifiable physiologic or histologic phenotypes in *Flk1^Cre^* and wild-type mice under normoxic conditions. Furthermore, we found no difference between wild-type, *Flk1^Cre^*, and *FGFR1^fl/fl^*; *FGFR2^fl/fl^* mice after challenge with hypoxia.

To rule out potential developmental and *Vegfr2* haploinsufficiency effects on the phenotype of FLK1-DCKO mice, we constructed Cdh5-DCKO mice as a second model to inducibly inactivate *Fgfr1* and *Fgfr2* in ECs in juvenile mice. Cdh5-DCKO mice did not show any apparent developmental or homeostatic defects under normoxic conditions. However, Cdh5-DCKO mice demonstrated worse PH when exposed to hypoxia, similar to but less severe than what was observed in FLK1-DCKO mice. These findings further support the model that EC FGFR signaling in adult mice worsens hypoxia-induced PH.

To test whether activation of EC FGFR signaling could protect against hypoxia-induced PH, we induced the expression of a chimeric constitutively active FGFR1 (caFGFR1) in ECs before and during exposure to hypoxia. Previously, we showed that caFGFR1 overexpression led to increased expression of downstream FGFR1 target signals and genes (44, 60, 61). Here, we showed that with caFGFR1 induced in ECs, the average RVp and RV hypertrophy of caFGFR1 mice were significantly lower than control littermates in hypoxia. In fact, the average RVp of the caFGFR1 group was comparable to that of normoxia controls. Additionally, histologic changes were limited to a moderate increase in VSM thickening of proximal, larger caliber vessels. Although *Tie2* also targets hematopoietic cell lineages, we did not observe any physiologic differences between control and caFGFR1 mice under normoxic conditions. As caFGFR1 expression was induced 2 weeks prior to and throughout the duration of hypoxia exposure, the absence of PH changes may, in part, be due to a preventive effect. To determine whether there may be a therapeutic effect of activated EC FGFR signaling, future studies will be required in which
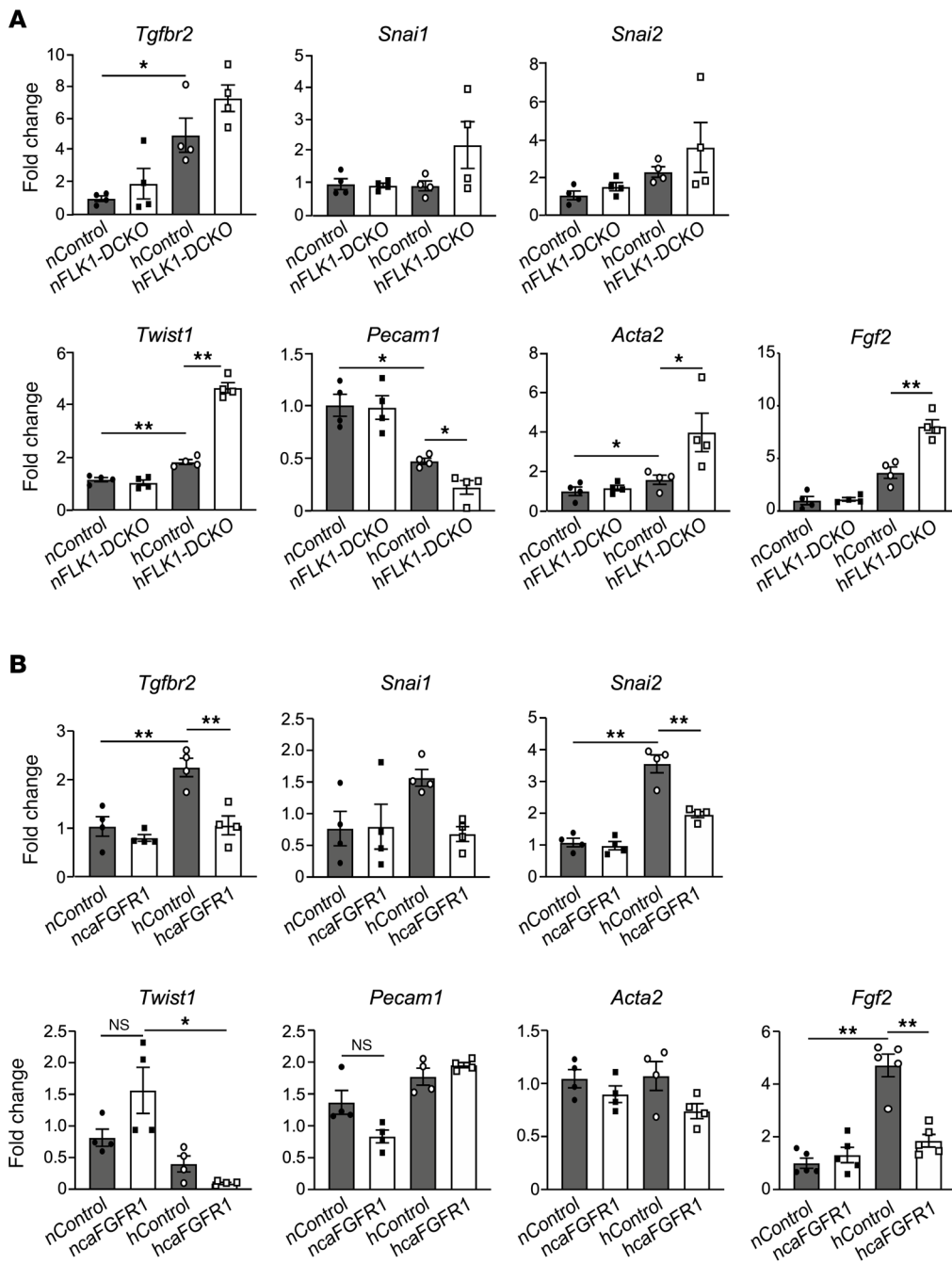
Figure 8. Effect of hypoxia and FGFR signaling on expression of the TGF-β–mediated endothelial-mesenchymal transition pathway. RNA expression of components of the TGF-β pathway during EndMT in lungs of hypoxia-exposed (**A**) FLK1-DCKO (n = 4) and (**B**) caFGFR1 mice (n = 4). Statistical significance was determined by 2-way ANOVA with Holm-Šídák multiple comparison test. All data are shown as the mean ± SEM. *P < 0.05, **P < 0.01. Closed circles, control mice in normoxia (nControl); open circles, control mice in hypoxia (hControl); closed squares, $Flk1^{Cre}$; $Fgfr1^{fl/fl}$; $Fgfr2^{fl/fl}$ mice in normoxia (nFLK1-DCKO) or caFGFR1 mice in normoxia (ncaFGFR1); open squares, $Flk1^{Cre}$; $Fgfr1^{fl/fl}$; $Fgfr2^{fl/fl}$ mice in hypoxia (hFLK1-DCKO) or caFGFR1 mice in hypoxia (hcaFGFR1).

caFGFR1 expression is induced at different time points after the initiation of hypoxia exposure.

We and others have reported that EC FGFR1 and FGFR2 are not necessary for vascular development or homeostasis, including the maintenance of normal vascular barrier function (39, 40, 41). Collectively, these studies suggest that under homeostatic conditions ECs are resistant to gain or loss of FGFR1/2 signaling. Further studies will be required to understand the basis of this resistance and how perturbations of homeostasis, such as injury or hypoxia, sensitize ECs to FGFR signaling. The absence of an effect of FGFR activation on unperturbed ECs also suggests that the EC FGFR1 signaling pathway may be a safe therapeutic target for the prevention of hypoxia-induced PH.

In contrast to the results in this study, Chang et al. showed that mice expressing perlecan that is deficient in heparan sulfate (HS), a cofactor for FGF-FGFR binding, have reduced PH in response to hypoxia (37). Although these mice may have reduced FGF signaling, several factors may account for their contrasting response to hypoxia. First, perlecan-HS may affect the activity of other growth factors in addition to FGF. For example, perlecan is required for VEGF signaling in skeletal angiogenesis, developmental angiogenesis, and VEGFR2 activation of human ECs (62, 63). Second, perlecan-HS–deficient mice have developmental defects that include a reduced percentage of αSMA-positive pulmonary vessels and reduced pericyte coverage of distal pulmonary vessels, which is in contrast with our EC-targeted FGFRs that have no change in
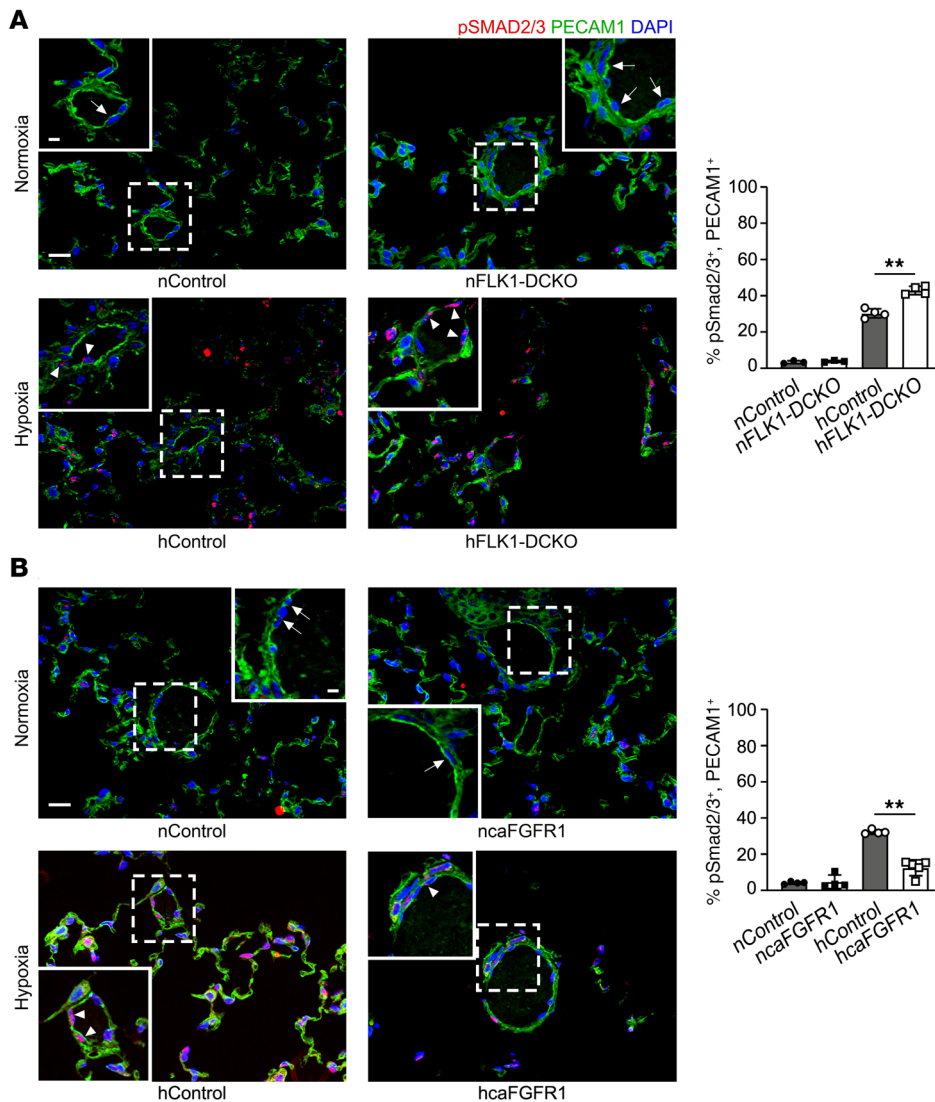
Figure 9. p-Smad2/3 expression in pulmonary endothelial cells. (**A** and **B**) Visualization of p-Smad2/3 (red) and endothelial cell (PECAM1, green) immunofluorescence. Arrowheads, p-Smad2/3+PECAM1+ double-positive endothelial cells; arrows, PECAM1+ singly positive endothelial cells. Scale bars: 25 μm and 20 μm (insets). Quantification of EndMT (right) showing the percentage p-SMAD2/3+PECAM1+ double-positive endothelial cells as a percentage of all PECAM1+ endothelial cells in (**A**) FLK1-DCKO and (**B**) caFGFR1 mouse lungs, respectively, *n* = 4. Statistical significance was determined by 2-way ANOVA with Holm-Šídák multiple comparison test. All data are shown as the mean ± SEM. **P < 0.01. Closed circles, control mice in normoxia (nControl); open circles, control mice in hypoxia (hControl); closed squares, *Flk1^Cre*; *Fgfr1^fl/fl*; *Fgfr2^fl/fl* mice in normoxia (nFLK1-DCKO) or caFGFR1 mice in normoxia (ncaFGFR1); open squares, *Flk1^Cre*; *Fgfr1^fl/fl*; *Fgfr2^fl/fl* mice in hypoxia (hFLK1-DCKO) or caFGFR1 mice in hypoxia (hcaFGFR1).

against hypoxia-induced PH. Fate mapping with reporter mice has facilitated the discovery of EndMT in many disease models. Qiao et al. found high levels of EC-lineage cells expressing αSMA and smooth muscle myosin heavy chain in remodeled pulmonary arteries of mice with PH (65). In the mouse models presented here, loss of EC FGFR signaling in vivo together with hypoxia exposure resulted in an increase in the number of smooth muscle cells of endothelial origin. Conversely, activation of FGFR signaling in ECs decreased the contribution of endothelium-originated cells to the smooth muscle layer, suggesting that FGFR signaling inhibits the EndMT process. Some of the EndMT processes include loss of EC cell-cell contact, increased expression of *Twist1*, *Snai1*, *Snai2*, and *Acta2*, and decreased expression of *Cdh5* and *Pecam1* (19, 20, 66). Hence, we show that exposing our mice to hypoxia increased expression *Tgfbr2* in vivo along with EndMT mediators *Snai1*, *Snai2*, and *Twist1*. We found that lack of EC FGFR signaling further augmented EndMT changes, and increased EC FGFR1 activity inhibited this process. FGF2 can modulate TGF-β1 signaling by regulating ALK5 and TGF-βR2 expression (67) and TWIST1 further enhances TGF-βR2 expression and Smad2 phosphorylation, resulting in decreased expression of EC markers (66, 68). Chen et al. also showed that inhibition of FGF signaling with a dominant negative mutant of FGFR1 or FRS2α increased TGF-β signaling (41). Hence, we asked whether EC FGFR activity modulates TGF-β signaling in hypoxia-exposed mice. We demonstrated that loss of EC FGFR and hypoxia exposure increased *Tgfbr2* expression and downstream *Twist1* expression. Consistent with these results, we showed that *Tgfbr2* expression was reduced when FGFR signaling was activated in the presence of hypoxia, resulting in decreased Smad2/3 phosphorylation. However, because FRS2 is also a critical regulator of VEGF signaling (69), further studies are warranted to determine the relative contributions of VEGFR and FGFR signaling to EndMT. Although the number of ECs expressing p-Smad2/3 in caFGFR1 mice was reduced, it remained slightly elevated compared with normoxia controls. This suggests that EC FGFR may
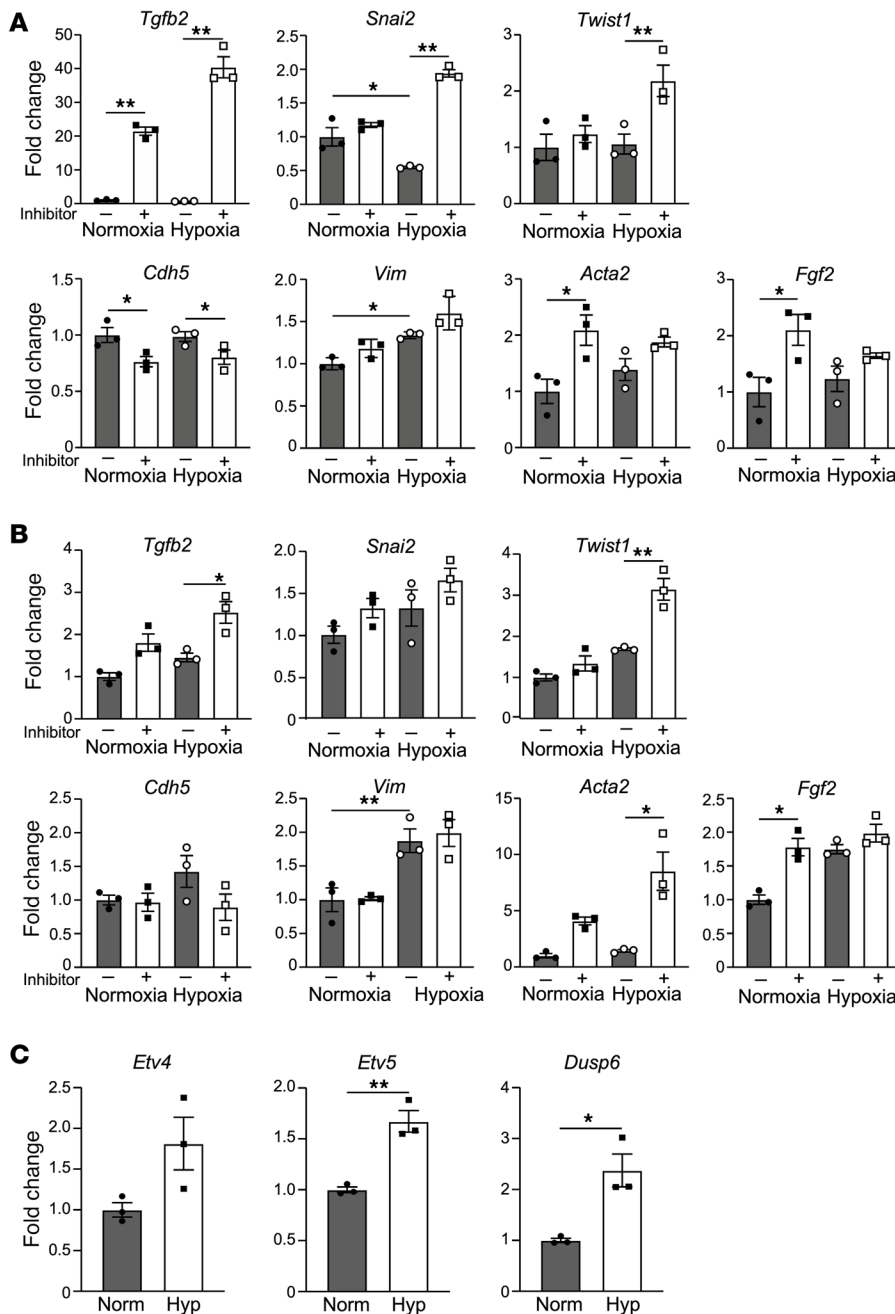
vascular wall thickening or neovascularization under normoxic conditions. Third, Chang et al. exposed female mice to 4 weeks of hypoxia, whereas we exposed male mice to 2 weeks of hypoxia, and we found a sex-specific difference in RVp when comparing male and female mice, with male mice showing lower RVp compared with female mice (Supplemental Figure 3).

EndMT is an adaptive response that is involved in the pathogenesis of several vascular diseases (21, 45, 64). Studies have shown that FGF-regulated TGF-β signaling can modulate EndMT in a mouse model of atherosclerosis (31). Hence, we hypothesized that EC FGFR signaling might reduce EndMT to protect

Figure 10. Effect of FGFR inhibition on genes involved in TGF-β–mediated endothelial-mesenchymal transition in human pulmonary artery endothelial cells (HPAECs). Relative RNA expression of components of the TGF-β pathway and mesenchymal markers during EndMT in HPAECs exposed to hypoxia for (**A**) 48 hours or (**B**) 14 days compared with controls in normoxia, with or without FGFR inhibitor BGJ398, *n* = 3. Statistical significance was determined by 2-way ANOVA with Holm-Šídák multiple comparison test. Closed circles, HPAECs in normoxia treated with vehicle; closed squares, HPAECs in normoxia treated with BGJ398; open circles, HPAECs in hypoxia treated with vehicle; open squares, HPAECs in hypoxia treated with BGJ398. (**C**) Relative RNA expression of *Fgf2* and downstream FGF signaling targets *Etv4*, *Etv5*, and *Dusp6* in HPAECs exposed to 14 days of hypoxia compared with controls in normoxia, *n* = 3. Statistical significance was determined by 2-tailed, unpaired Student's *t* test. *$P < 0.01$, **$P < 0.05$. All data are shown as the mean ± SEM.

only partially suppress TGF-β signaling, but that this is sufficient for PH phenotype rescue. SNAI1 and SNAI2 are known to mediate hypoxia-induced EndMT (70) and combined SNAI1 overexpression and TGF-β2 treatment markedly induced EndMT, resulting in endothelial and mesenchymal marker changes along with EC migration (71). In support of our findings that FGFR signaling regulated *Snai1* and *Snai2* expression, Cooley et al. and Medici et al. showed the EndMT is regulated by a TGF-β–activated Smad2/3/SNAI2–dependent signaling pathway (72, 73). Collectively, our in vivo expression data show that FGFR signaling regulates the TGF-β/SMAD pathway–dependent expression of downstream EndMT mediators. We noted that the lack of change in *Pecam1* and *Acta2* expression in doxycycline-treated hypoxia-exposed mice and their normoxia littermates may be due to the effect of

doxycycline treatment, which increased VE-cadherin expression to enhance EC adherens junctions (74).

TGF-β signaling has been shown to regulate EndMT in ECs in vitro (29, 45) and inhibition of FGF signaling together with TGF-β stimulation can augment Smad2/3 phosphorylation (75). Thus, we asked whether TGF-β signaling was affected by gain or loss of EC FGF signaling in HPAECs cultured under hypoxic conditions. First, we showed that short-term (48 hour) inhibition of FGFR signaling increased *Tgfb2* expression in normoxia but had no effect on downstream signaling components. In the presence of hypoxia, FGFR inhibition with BGJ398 increased expression of *Tgfb2* and downstream mediators and markers of EndMT. To determine the effect of FGF inhibition on chronic hypoxia, we exposed HPAECs to 14 days of hypoxia and showed that prolonged hypoxia increased
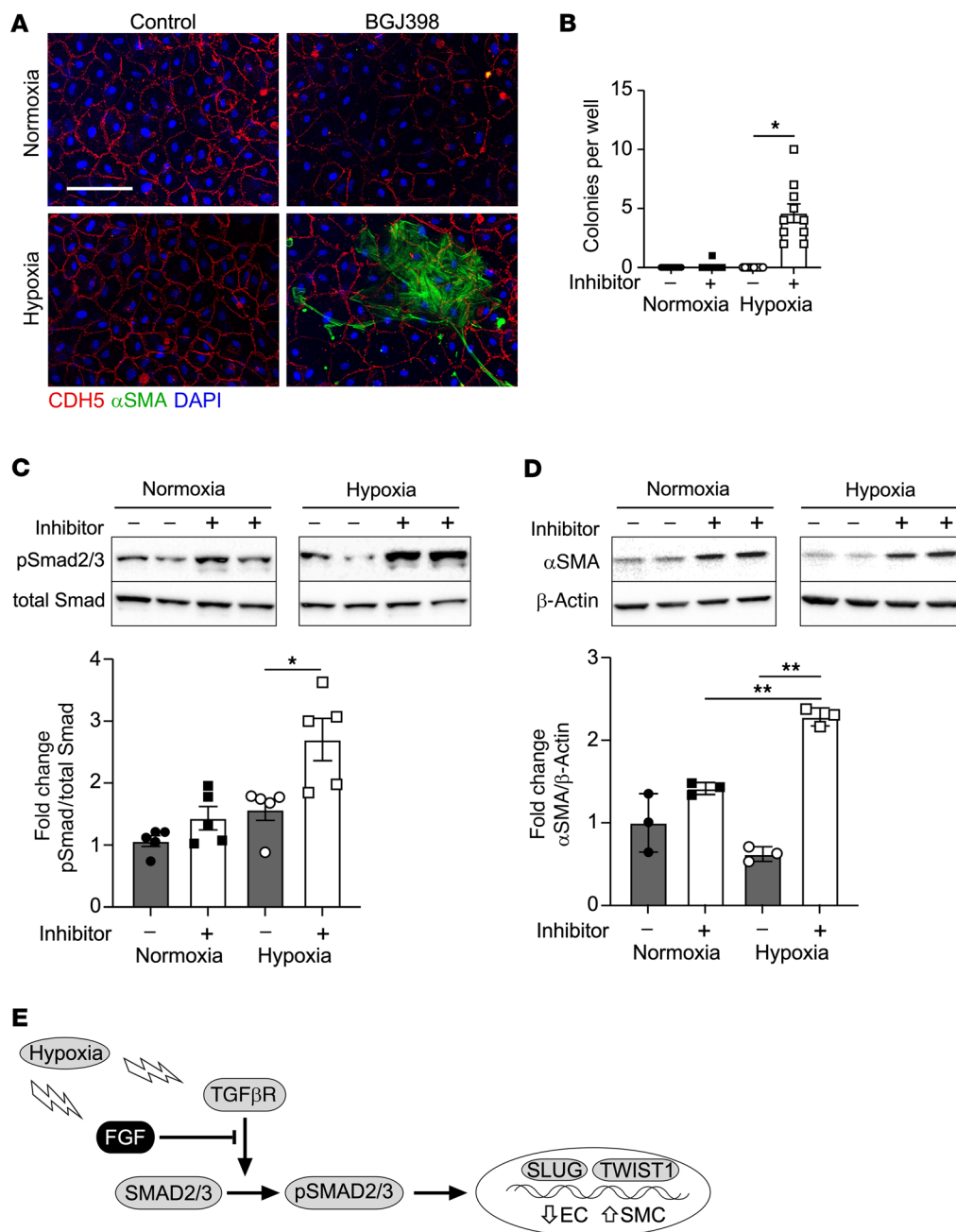
Figure 11. Effect of FGFR inhibition on endothelial-mesenchymal transition in human pulmonary artery endothelial cells (HPAECs). (**A**) Representative images of CDH5 (red) and αSMA (green) immunofluorescence in HPAECs treated with FGFR inhibitor BGJ398 under hypoxic conditions compared with controls in normoxia. Scale bar: 10 μm. (**B**) Quantification of the number of colonies of αSMA-positive cells per culture well in HPAECs treated with the FGFR inhibitor BGJ398 under hypoxic conditions compared with controls in normoxia, n = 4–10. Closed circles, HPAECs in normoxia treated with vehicle; open circle, HPAECs in hypoxia treated with vehicle; closed squares, HPAECs in normoxia treated with inhibitor; open squares, HPAECs in hypoxia treated with inhibitor. (**C**) Representative Western blots and quantification of p-Smad2/3 normalized to total Smad proteins, n = 5. (**D**) Representative Western blots and quantification of αSMA normalized to β-actin, n = 3. See complete unedited blots in the supplemental material. Statistical significance was determined by 2-way ANOVA with Holm-Šídák multiple comparison test. All data are shown as the mean ± SEM. *P < 0.05, **P < 0.01. (**E**) Proposed model showing FGF inhibition of hypoxia-stimulated TGF-β signaling in endothelial-mesenchymal transition.

Smad2/3 phosphorylation and elevated EndMT mediators. Notably, we found that *Fgf2* and its downstream targets *Etv4*, *Etv5*, and *Dusp6* were also elevated after 14 days of hypoxia, suggesting a negative feedback mechanism of FGF signaling during EndMT. DUSP6 is a negative feedback regulator of FGFR signaling (76, 77) and is also known to regulate EC inflammation via NF-κB–mediated ICAM-1 expression (78). This would suggest that the increased DUSP6 expression is a pro-EndMT response to hypoxia to negatively regulate FGFR signaling and activate the EC inflammatory process. Previous studies demonstrated EndMT in vitro after 3–4 days of hypoxia with human coronary artery ECs (79) and less than 24 hours of hypoxia with bovine aortic ECs (24). In our system, we observed colonies of αSMA-expressing cells among HPAECs, indicating EndMT in vitro after 2 weeks of hypoxia. Although primary

ECs can transdifferentiate in vitro when cultured on plastic or glass, we did not detect this in our cultures. This may be due to several factors: HPAECs were cultured on gelatin-coated dishes using EC growth media, and dishes were subcultured at lower density to optimize for 80%–100% confluence at the end of 2 weeks. We observed that HPAECs that had undergone EndMT were localized in colonies spread out across the dish. Further studies would need to be conducted to determine if each colony was clonally propagated. Collectively, these data show that, with FGF inhibition, HPAECs cultured in prolonged hypoxia can undergo EndMT.

To evaluate whether EndMT occurs in pulmonary conditions that may contribute to Group 3 PH, we assessed lung samples from patients with CPFE with documented elevated mean pulmonary artery pressure (mPAP > 25 mmHg). We noted decreased
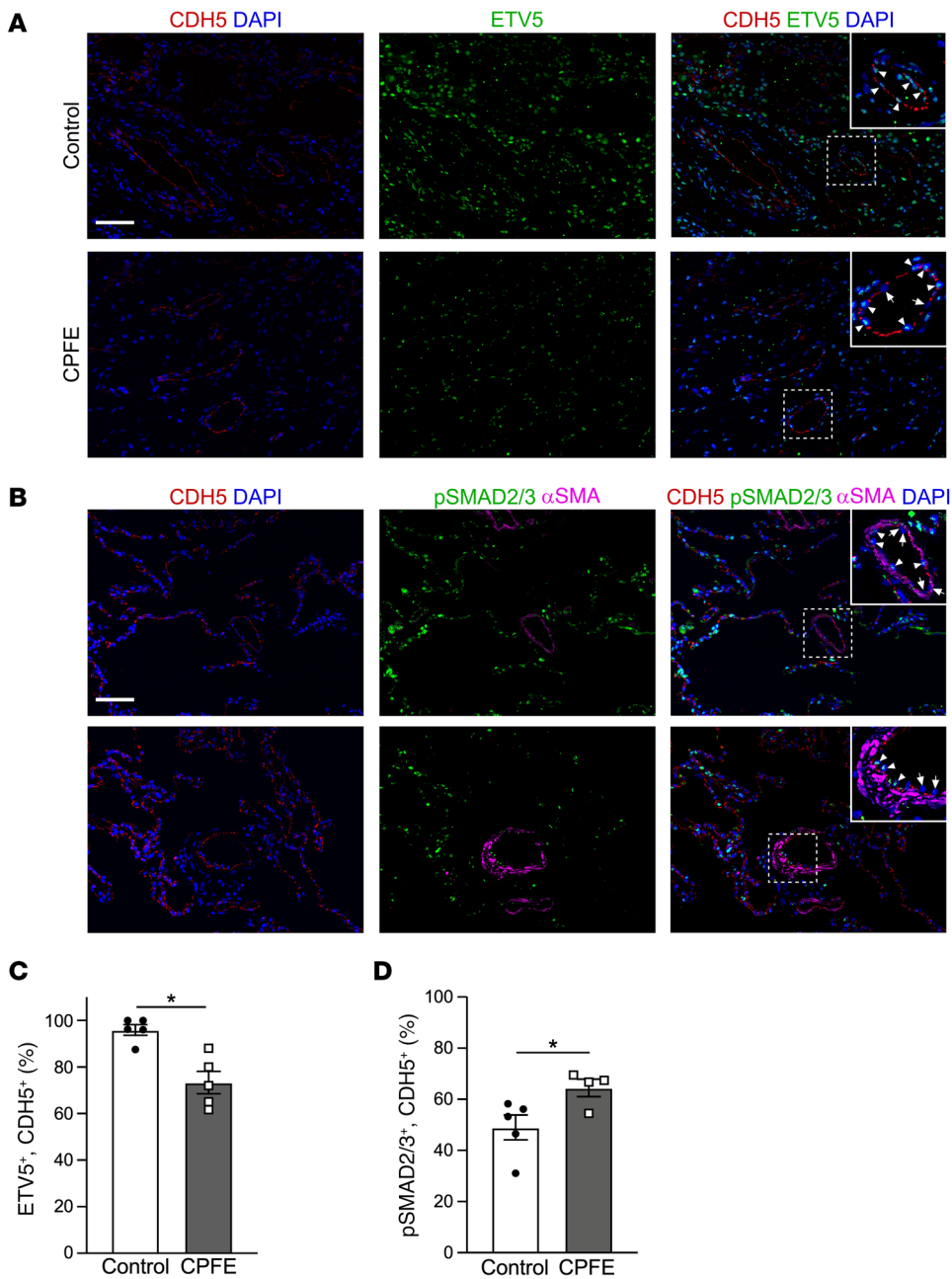
Figure 12. FGF signaling in lungs of patients with combined pulmonary fibrosis and emphysema. (**A**) Representative immunofluorescence images showing expression of ETV5 (green) and CDH5 (red) in endothelial cells in lung tissue from patients with CPFE compared with normal lung tissue (control). Arrowheads, ETV5⁺CDH5⁺ double-positive endothelial cells; arrows, CDH5⁺ singly positive endothelial cells. Scale bars: 25 μm and 20 μm (insets). (**B**) Representative immunofluorescence images showing p-Smad2/3 (green) and CDH5 (red) expression in endothelial cells in lung tissue from patients with CPFE compared with normal lung tissue (control). Arrowheads, p-SMAD2/3⁺CDH5⁺ double-positive endothelial cells; arrows, CDH5⁺ singly positive endothelial cells. Scale bars: 5 μm and 20 μm (insets). (**C**) Quantification of ETV5⁺CDH5⁺ double-positive endothelial cells in CPFE compared with control lungs, n = 5. (**D**) Quantification of p-SMAD2/3⁺CDH5⁺ double-positive endothelial cells in CPFE compared with control lungs, n = 5. Statistical significance was determined by 2-tailed, unpaired Student's t test. *P < 0.05. All data are shown as the mean ± SEM.

FGFR signaling and increased TGF-β signaling in lung tissue from these patients. These data are consistent with our mouse model and in vitro experiments suggesting that activation of FGFR signaling inhibits TGF-β signaling–induced EndMT. Collectively, these studies support a model in which FGFR signaling modulates hypoxia-induced EndMT, at least in part, by regulating TGF-β/SMAD2/3 signaling (Figure 11E).

Expression of *Fgf2* is increased after chronic hypoxia in vivo in mouse and patient samples and in vitro in HPAECs. In CPFE patients with physiologic changes consistent with PH, we noted decreased FGFR signaling. Yet, we also showed that constitutive FGFR1 signaling leads to reduced PH in mice. Although there was no PH in hypoxia-exposed caFGFR1 mice, we still observed increased vascular wall thickening in the larger proximal vessels (Figure 5C), consistent with moderately increased p-Smad2/3

and EndMT. This suggests that TGF-β–mediated EndMT is only partially regulated by EC-caFGFR1 signaling or that other factors independent of EndMT contribute to vascular wall thickening in response to hypoxia.

Our studies show that loss of FGFR signaling in the endothelium results in more severe Group 3 hypoxia-induced PH, which is in contrast to studies on Group 1 PH (PAH) that suggest that FGFR signaling is pathologic (33, 34, 36) and that inhibition of FGF2 activity is beneficial (33–35). Pulmonary ECs from PAH patients (PAH-ECs) exhibited higher FGF2 expression (34), increased FGF2 in the culture media, and increased survival and proliferation when treated with exogenous FGF2 (33). When treated with PAH-EC–conditioned culture media, smooth muscle cells from PAH patients demonstrated increased proliferation (36). Downregulation of Apelin, miR-424, and

miR-503 in PAH-ECs increased FGF2 and FGFR1 expression and pulmonary artery EC and VSM cell proliferation (35). Using the monocrotaline-induced model of PH in rats, Izikki et al. showed that 2 treatments with the VEGFR2 and FGFR1 inhibitor SU5402 reversed the PH effects (34). Our data showing that FGFR signaling is protective against hypoxia-induced PH suggests a divergent role for FGF signaling in a disease context–dependent manner. However, these differences may also be due to the different animal models and that PAH-ECs may already be sensitized to PH changes compared with HPAECs isolated from normal lungs.

Hypoxia augments the Kruppel-like factor 4–dependent (KLF4-dependent) clonal expansion of VSM progenitors in pulmonary arterioles (80). Increased FGF2 expression in PAH-EC–conditioned media augments VSM cell proliferation (35). We showed that, after hypoxia exposure, FGF2 expression is increased in FLK1-DCKO mice and decreased in caFGFR1 mice. FGF-regulated EndMT in hypoxia-exposed ECs may play a partial role in contributing to increased VSM in the medial layer. Increased paracrine FGF2 expression may play a direct role in VSM cell proliferation. Further studies will be needed to determine the role of FGF signaling in chronic hypoxia–induced VSM cell proliferation.

We recognize that assessment of gene expression with RNA generated from whole lungs of hypoxia-exposed mice is a limitation of this study. We considered fluorescence-assisted cell sorting to isolate ECs; however, the tissue would be exposed to normoxic conditions for several hours during tissue digestion and cell sorting, and this process would not assess regional differences in ECs. Furthermore, EC FGF2 expression is amplified by a HIF1α-dependent pathway (38), and chronic but not short-term hypoxic induction of HIF1α in HUVECs is FGF2 dependent. Further studies are needed to investigate the role of FGF2-HIF1α interactions during EndMT under chronic hypoxic conditions. Because FGF2-HIF1α crosstalk can mediate angiogenesis in tumor models (81), additional studies will be needed to determine whether chronic hypoxia induces a similar FGF-HIF1α signaling interaction.

These findings may have important clinical implications for preclinical and clinical studies aimed at preventing patients at risk from developing chronic hypoxia-induced PH or treating patients with hypoxia-induced PH. There is a growing recognition of the clinical importance of hypoxic lung disease. The observation that endogenous FGFR signaling may limit the progression of hypoxia-induced PH and that further activation of EC FGFR signaling may prevent key pathological features of hypoxia-induced PH opens potential avenues to explore biological therapies for this family of diseases.

Methods

Animal care and use. Mice were group housed in a specific pathogen–free facility with littermates, in breeding pairs, or in a breeding harem (2 females to 1 male), with food and water provided ad libitum.

Study approval. All studies performed were in accordance with the Institutional Animal Care and Use Committee at Washington University in St. Louis (protocol nos. 20160113 and 20190110). Mice were handled in accordance with standard use protocols, animal welfare regulations, and the NIH *Guide for the Care and Use of Laboratory Animals* (National Academies Press, 2011).

All human participants consented to donate their lung tissues for research under protocols approved by the Washington University Institutional Review Board (98-0510/201103213). Patient identifiers including name, age, sex, and ethnic group were concealed.

Author contributions

Acknowledgments

Address correspondence to: David Ornitz, 3905 South Bldg, Washington University School of Medicine, 660 S. Euclid Avenue, St. Louis, Missouri 63110, USA. Email: dornitz@wustl.edu.

1. Simonneau G, et al. Updated clinical classification of pulmonary hypertension. *J Am Coll Cardiol*. 2009;54(1 suppl):S43–S54.
2. Badesch DB, et al. Pulmonary arterial hypertension: baseline characteristics from the REVEAL Registry. *Chest*. 2010;137(2):376–387.
3. Stoll BJ, et al. Neonatal outcomes of extremely preterm infants from the NICHD Neonatal Research Network. *Pediatrics*. 2010;126(3):443–456.
4. Oswald-Mammosser M, et al. Prognostic factors in COPD patients receiving long-term oxygen therapy. Importance of pulmonary artery pressure. *Chest*. 1995;107(5):1193–1198.
5. Girard N, et al. Chemotherapy is the cornerstone of the combined surgical treatment of lung cancer with synchronous brain metastases. *Lung Cancer*. 2006;53(1):51–58.
6. Seeger W, et al. Pulmonary hypertension in chronic lung diseases. *J Am Coll Cardiol*. 2013;62(25 suppl):D109–D116.

7. Cottin V, et al. Combined pulmonary fibrosis and emphysema: a distinct underrecognised entity. *Eur Respir J*. 2005;26(4):586–593.

8. Cottin V, et al. Pulmonary hypertension in patients with combined pulmonary fibrosis and emphysema syndrome. *Eur Respir J*. 2010;35(1):105–111.

9. Caminati A, et al. Pulmonary hypertension in chronic interstitial lung diseases. *Eur Respir Rev*. 2013;22(129):292–301.

10. Lin H, Jiang S. Combined pulmonary fibrosis and emphysema (CPFE): an entity different from emphysema or pulmonary fibrosis alone. *J Thorac Dis*. 2015;7(4):767–779.

11. Stenmark KR, et al. Hypoxia-induced pulmonary vascular remodeling: cellular and molecular mechanisms. *Circ Res*. 2006;99(7):675–691.

12. Durmowicz AG, Stenmark KR. Mechanisms of structural remodeling in chronic pulmonary hypertension. *Pediatr Rev*. 1999;20(11):e91–e102.

13. Michiels C, et al. Endothelial cell responses to hypoxia: initiation of a cascade of cellular interactions. *Biochim Biophys Acta*. 2000;1497(1):1–10.

14. Sakao S, et al. Endothelial cells and pulmonary arterial hypertension: apoptosis, proliferation, interaction and transdifferentiation. *Respir Res*. 2009;10:95.

15. Estrada KD, Chesler NC. Collagen-related gene and protein expression changes in the lung in response to chronic hypoxia. *Biomech Model Mechanobiol*. 2009;8(4):263–272.

16. Cohen JL, et al. Sildenafil use in children with pulmonary hypertension. *J Pediatr*. 2019;205:29–34.

17. Mourani PM, et al. Effects of long-term sildenafil treatment for pulmonary hypertension in infants with chronic lung disease. *J Pediatr*. 2009;154(3):379–384.

18. Leopold JA, Maron BA. Molecular mechanisms of pulmonary vascular remodeling in pulmonary arterial hypertension. *Int J Mol Sci*. 2016;17(5):E761.

19. Sanchez-Duffhues G, et al. Endothelial-to-mesenchymal transition in cardiovascular diseases: developmental signaling pathways gone awry. *Dev Dyn*. 2018;247(3):492–508.

20. Good RB, et al. Endothelial to mesenchymal transition contributes to endothelial dysfunction in pulmonary arterial hypertension. *Am J Pathol*. 2015;185(7):1850–1858.

21. Stenmark KR, et al. Endothelial-to-mesenchymal transition: an evolving paradigm and a promising therapeutic target in PAH. *Circulation*. 2016;133(18):1734–1737.

22. Perez L, et al. Endothelial-to-mesenchymal transition: Cytokine-mediated pathways that determine endothelial fibrosis under inflammatory conditions. *Cytokine Growth Factor Rev*. 2017;33:41–54.

23. Massague J. TGF-beta signal transduction. *Annu Rev Biochem*. 1998;67:753–791.

24. Doerr M, et al. Differential effect of hypoxia on early endothelial-mesenchymal transition response to transforming growth beta isoforms 1 and 2. *Microvasc Res*. 2016;108:48–63.

25. Cano A, et al. The transcription factor snail controls epithelial-mesenchymal transitions by repressing E-cadherin expression. *Nat Cell Biol*. 2000;2(2):76–83.

26. Bolos V, et al. The transcription factor Slug represses E-cadherin expression and induces epithelial to mesenchymal transitions: a comparison with Snail and E47 repressors. *J Cell Sci*. 2003;116(pt 3):499–511.

27. Yang J, et al. Twist, a master regulator of morphogenesis, plays an essential role in tumor metastasis. *Cell*. 2004;117(7):927–939.

28. Teng Y, Li X. The roles of HLH transcription factors in epithelial mesenchymal transition and multiple molecular mechanisms. *Clin Exp Metastasis*. 2014;31(3):367–377.

29. Xiao L, et al. Tumor endothelial cells with distinct patterns of TGFβ-driven endothelial-to-mesenchymal transition. *Cancer Res*. 2015;75(7):1244–1254.

30. Peinado H, et al. Snail, Zeb and bHLH factors in tumour progression: an alliance against the epithelial phenotype? *Nat Rev Cancer*. 2007;7(6):415–428.

31. Chen PY, et al. FGF regulates TGF-β signaling and endothelial-to-mesenchymal transition via control of let-7 miRNA expression. *Cell Rep*. 2012;2(6):1684–1696.

32. Hopper RK, et al. In pulmonary arterial hypertension, reduced BMPR2 promotes endothelial-to-mesenchymal transition via HMGA1 and its target slug. *Circulation*. 2016;133(18):1783–1794.

33. Tu L, et al. Autocrine fibroblast growth factor-2 signaling contributes to altered endothelial phenotype in pulmonary hypertension. *Am J Respir Cell Mol Biol*. 2011;45(2):311–322.

34. Izikki M, et al. Endothelial-derived FGF2 contributes to the progression of pulmonary hypertension in humans and rodents. *J Clin Invest*. 2009;119(3):512–523.

35. Kim J, et al. An endothelial apelin-FGF link mediated by miR-424 and miR-503 is disrupted in pulmonary arterial hypertension. *Nat Med*. 2013;19(1):74–82.

36. Gore B, et al. Key role of the endothelial TGF-β/ALK1/endoglin signaling pathway in humans and rodents pulmonary hypertension. *PLoS One*. 2014;9(6):e100310.

37. Chang YT, et al. Perlecan heparan sulfate deficiency impairs pulmonary vascular development and attenuates hypoxic pulmonary hypertension. *Cardiovasc Res*. 2015;107(1):20–31.

38. Calvani M, et al. Hypoxic induction of an HIF-1alpha-dependent bFGF autocrine loop drives angiogenesis in human endothelial cells. *Blood*. 2006;107(7):2705–2712.

39. House SL, et al. Endothelial fibroblast growth factor receptor signaling is required for vascular remodeling following cardiac ischemia-reperfusion injury. *Am J Physiol Heart Circ Physiol*. 2016;310(5):H559–H571.

40. Oladipupo SS, et al. Endothelial cell FGF signaling is required for injury response but not for vascular homeostasis. *Proc Natl Acad Sci U S A*. 2014;111(37):13379–13384.

41. Chen PY, et al. Fibroblast growth factor receptor 1 is a key inhibitor of TGFβ signaling in the endothelium. *Sci Signal*. 2014;7(344):ra90.

42. Xiao L, Dudley AC. Fine-tuning vascular fate during endothelial-mesenchymal transition. *J Pathol*. 2017;241(1):25–35.

43. Thibault HB, et al. Noninvasive assessment of murine pulmonary arterial pressure: validation and application to models of pulmonary hypertension. *Circ Cardiovasc Imaging*. 2010;3(2):157–163.

44. Cilvik SN, et al. Fibroblast growth factor receptor 1 signaling in adult cardiomyocytes increases contractility and results in a hypertrophic cardiomyopathy. *PLoS One*. 2013;8(12):e82979.

45. Chen PY, et al. Endothelial-to-mesenchymal transition drives atherosclerosis progression. *J Clin Invest*. 2015;125(12):4514–4528.

46. Presta M, et al. Fibroblast growth factor/fibroblast growth factor receptor system in angiogenesis. *Cytokine Growth Factor Rev*. 2005;16(2):159–178.

47. Claus P, Grothe C. Molecular cloning and developmental expression of rat fibroblast growth factor receptor 3. *Histochem Cell Biol*. 2001;115(2):147–155.

48. Shin JW, et al. Prox1 promotes lineage-specific expression of fibroblast growth factor (FGF) receptor-3 in lymphatic endothelium: a role for FGF signaling in lymphangiogenesis. *Mol Biol Cell*. 2006;17(2):576–584.

49. Dong Z, et al. FGF2-induced STAT3 activation regulates pathologic neovascularization. *Exp Eye Res*. 2019;187:107775.

50. Das M, et al. A process-based review of mouse models of pulmonary hypertension. *Pulm Circ*. 2012;2(4):415–433.

51. Kobs RW, et al. Linked mechanical and biological aspects of remodeling in mouse pulmonary arteries with hypoxia-induced hypertension. *Am J Physiol Heart Circ Physiol*. 2005;288(3):H1209–H1217.

52. Netto D, Vladutiu AO. A simple technique for identification of "unreactive" light chains of immunoglobulins. *Clin Chim Acta*. 1981;116(2):253–260.

53. Thirunavukkarasu M, et al. Heterozygous disruption of Flk-1 receptor leads to myocardial ischaemia reperfusion injury in mice: application of affymetrix gene chip analysis. *J Cell Mol Med*. 2008;12(4):1284–1302.

54. Voelkel NF, Gomez-Arroyo J. The role of vascular endothelial growth factor in pulmonary arterial hypertension. The angiogenesis paradox. *Am J Respir Cell Mol Biol*. 2014;51(4):474–484.

55. Ciuclan L, et al. A novel murine model of severe pulmonary arterial hypertension. *Am J Respir Crit Care Med*. 2011;184(10):1171–1182.

56. Van Hung T, et al. Inhibition of vascular endothelial growth factor receptor under hypoxia causes severe, human-like pulmonary arterial hypertension in mice: potential roles of interleukin-6 and endothelin. *Life Sci*. 2014;118(2):313–328.

57. Tessneer KL, et al. Genetic reduction of vascular endothelial growth factor receptor 2 rescues aberrant angiogenesis caused by epsin deficiency. *Arterioscler Thromb Vasc Biol*. 2014;34(2):331–337.

58. Oladipupo SS, et al. Impaired tumor growth and angiogenesis in mice heterozygous for Vegfr2 (Flk1). *Sci Rep*. 2018;8(1):14724.

59. Karaman S, et al. Vascular endothelial growth factor signaling in development and disease. *Development*. 2018;145(14):dev151019.

60. Huh SH, et al. Cochlear progenitor number is controlled through mesenchymal FGF receptor signaling. *Elife*. 2015;4:e05921.

61. BonDurant LD, et al. FGF21 regulates metabolism through adipose-dependent and -independent mechanisms. *Cell Metab*. 2017;25(4):935–944.

62. Sano T, et al. Complete nucleotide sequence of a viroid isolated from Etrog citron, a new member of hop stunt viroid group. *Nucleic Acids Res*. 1988;16(1):347.

63. Burns DK, Beaumont PL. The HSE national exposure database--(NEDB). *Ann Occup Hyg*. 1989;33(1):1–14.

64. Chen PY, Simons M. Fibroblast growth factor-transforming growth factor beta dialogues, endothelial cell to mesenchymal transition, and atherosclerosis. *Curr Opin Lipidol*. 2018;29(5):397–403.

65. Qiao L, et al. Endothelial fate mapping in mice with pulmonary hypertension. *Circulation*. 2014;129(6):692–703.

66. Ranchoux B, et al. Endothelial-to-mesenchymal transition in pulmonary hypertension. *Circulation*. 2015;131(11):1006–1018.

67. Correia AC, et al. FGF2 inhibits endothelial-mesenchymal transition through microRNA-20a-mediated repression of canonical TGF-β signaling. *J Cell Sci*. 2016;129(3):569–579.

68. Kwapiszewska G, et al. A twist on pulmonary vascular remodeling: endothelial to mesen-chymal transition? *Am J Respir Cell Mol Biol*. 2018;58(2):140–141.

69. Hassan AK, el Tom K. Combined natural infection with infectious bovine rhinotracheitis and rinderpest viruses. *Trop Anim Health Prod*. 1985;17(1):52.

70. Tang H, et al. Endothelial HIF-2α contributes to severe pulmonary hypertension due to endothelial-to-mesenchymal transition. *Am J Physiol Lung Cell Mol Physiol*. 2018;314(2):L256–L275.

71. Pinto MT, et al. Endothelial cells from different anatomical origin have distinct responses during SNAIL/TGF-beta2-mediated endothelial-mesenchymal transition. *Am J Transl Res*. 2018;10(12):4065–4081.

72. Cooley BC, et al. TGF-β signaling mediates endothelial-to-mesenchymal transition (EndMT) during vein graft remodeling. *Sci Transl Med*. 2014;6(227):227ra34.

73. Medici D, et al. Transforming growth factor-β2 promotes Snail-mediated endothelial-mesenchymal transition through convergence of Smad-dependent and Smad-independent signalling. *Biochem J*. 2011;437(3):515–520.

74. Fainaru O, et al. Doxycycline inhibits vascular leakage and prevents ovarian hyperstimulation syndrome in a murine model. *Fertil Steril*. 2009;92(5):1701–1705.

75. Chen PY, et al. Fibroblast growth factor (FGF) signaling regulates transforming growth factor beta (TGFβ)-dependent smooth muscle cell phenotype modulation. *Sci Rep*. 2016;6:33407.

76. Ornitz DM, Itoh N. The fibroblast growth factor signaling pathway. *Wiley Interdiscip Rev Dev Biol*. 2015;4(3):215–266.

77. Li C, et al. Dusp6 (Mkp3) is a negative feedback regulator of FGF-stimulated ERK signaling during mouse development. *Development*. 2007;134(1):167–176.

78. Hsu SF, et al. Dual specificity phosphatase DUSP6 promotes endothelial inflammation through inducible expression of ICAM-1. *FEBS J*. 2018;285(9):1593–1610.

79. Xu YP, et al. MiR-126a-5p is involved in the hypoxia-induced endothelial-to-mesenchymal transition of neonatal pulmonary hypertension. *Hypertens Res*. 2017;40(6):552–561.

80. Sheikh AQ, et al. Smooth muscle cell progenitors are primed to muscularize in pulmonary hypertension. *Sci Transl Med*. 2015;7(308):308ra159.

81. Conte C, et al. FGF2 translationally induced by hypoxia is involved in negative and positive feedback loops with HIF-1alpha. *PLoS One*. 2008;3(8):e3078.